SECOND EDITION

SATELLITE COMMUNICATIONS SYSTEMS ENGINEERING

Atmospheric Effects, Satellite Link Design and System Performance

LOUIS J. IPPOLITO JR.

WILEY

www.EngineeringBooksPdf.com

6

Transmission Impairments

The influence of the earth's atmosphere on radiowaves propagating between earth and space is a constant concern in the design and performance of satellite communications systems. These conditions, when present alone or in combination on the earth-space link, can cause uncontrolled variations in signal amplitude, phase, polarization, and angle of arrival, which result in a reduction in the quality of analog transmissions and an increase in the error rate of digital transmissions.

The relative importance of radiowave propagation in space communications depends on the frequency of operation, local climatology, local geography, type of transmission, and elevation angle to the satellite. Generally, the effects become more significant as the frequency increases and as the elevation angle decreases. The random nature and general unpredictability of the phenomena that produce the propagation effects add further dimensions of complexity and uncertainty in the evaluation of transmission impairments on satellite communications. Consequently, statistical analyses and techniques are generally most useful for evaluation of transmission impairments on communications links [1].

6.1 Radiowave Frequency and Space Communications

The frequency of the radiowave is a critical factor in determining whether impairments to space communications will be introduced by the Earth's atmosphere. Figure 6.1 shows the elements of Earth's atmosphere that impact radiowave communications on space communications. A radiowave will propagate from the Earth's surface to outer space provided its frequency is high enough to penetrate the ***ionosphere***, which is the ionized region extending from about 15 km to roughly 400 km above the surface. The various regions (or layers) in the ionosphere, designated D, E, and F, in order of increasing altitude (see right side of Figure 6.1), act as reflectors or absorbers to radiowaves at frequencies below about 30 MHz, and space communications is not possible. As the operating frequency is increased, the reflection properties of the E and F layers are reduced and the signal will propagate through. Radiowaves above about 30 MHz will propagate through the ionosphere, however, the properties of the wave could be modified or degraded to varying degrees depending on frequency, geographic location, and time of day. Ionospheric effects tend to become less significant as the frequency of the wave increases, and above about 3 GHz the ionosphere is essentially transparent to space communications, with some notable exceptions, which will be discussed later.

Satellite Communications Systems Engineering: Atmospheric Effects, Satellite Link Design and System Performance, Second Edition. Louis J. Ippolito, Jr.
© 2017 John Wiley & Sons Ltd. Published 2017 by John Wiley & Sons Ltd.
www.EngineeringBooksPdf.com

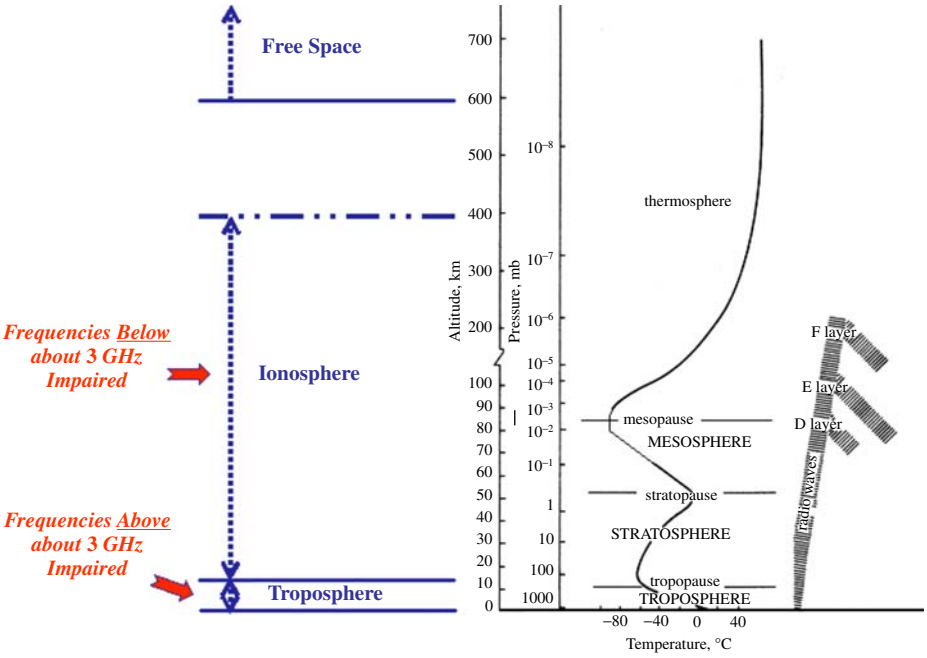

Figure 6.1 Components of the atmosphere impacting space communications.

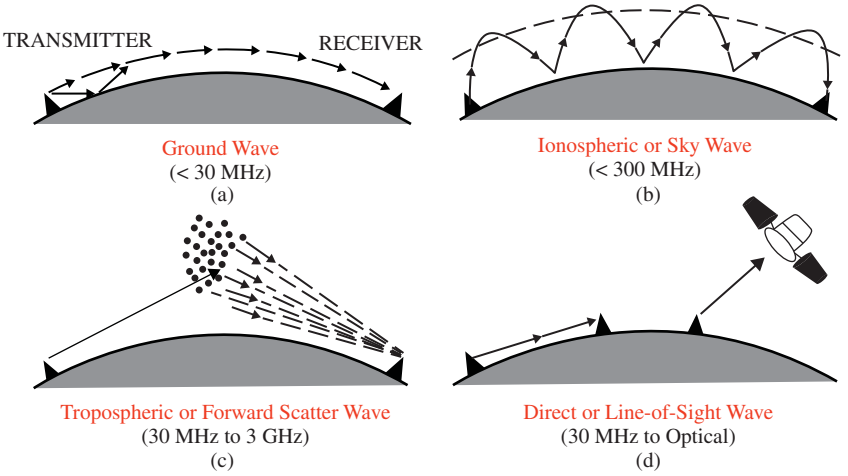

Figure 6.2 Radiowave propagation modes. (Source: Ippolito [1]; reproduced by permission of Van Nostrand Reinhold.)

Several types of radiowave propagation modes can be generated in the Earth's atmosphere, depending on transmission frequency and other factors. Below the ionospheric penetration frequency, a radiowave will propagate along the Earth's surface, as illustrated in Figure 6.2(a). This mode is defined as ground wave propagation, and consists of three components; a direct wave, a ground reflected wave, and a surface

www.EngineeringBooksPdf.com

wave, which is guided along the Earth's surface. This mode supports broadcasting and communications services, such as the AM broadcast band, amateur radio, radio navigation, and land mobile services.

A second type of terrestrial propagation mode, called an ionospheric or sky wave, can also be supported under certain ionospheric conditions, as shown in Figure 6.2(b). In this mode, which occurs at frequencies below about 300 MHz, the wave propagates toward and returns from the ionosphere, "hopping" along the surface of the Earth. This frequency range includes the commercial FM and VHF television bands as well as aeronautical and marine mobile services.

Above about 30 MHz, and up to about 3 GHz, reliable long distance over the horizon communications can be generated by a scattering of energy from refractive index irregularities in the troposphere, the region from the Earth's surface up to about 10 20 Km in altitude. This mode of propagation, termed a tropospheric or forward scattered wave [see Figure 6.2(c)], is highly variable and is subject to intense fluctuations and interruptions. This mode has been and is being used, however, for long distance communications when no other means are available.

Tropospheric scatter propagation can also be a factor in space communications when the scattered signal from a ground transmitter interferes with a ground receiver operating in the same frequency band. The scattered signal will appear as noise in the receiver and can directly contribute to degradation in system performance.

Finally, at frequencies well above the ionospheric penetration frequency, direct or line of sight propagation predominates, and this is the primary mode of operation for space communications [see Figure 6.2(d)]. Terrestrial radio relay communications and broadcasting services also operate in this mode, often sharing the same frequency bands as the space services.

Line of sight space communications will continue unimpeded as the frequency of transmission is increased up to frequencies where the gaseous constituents of the troposphere, primarily oxygen and water vapor, will absorb energy from the radiowave. At certain specific ***absorption bands***, where the radiowave and gaseous interaction are particularly intense, space communications are severely limited. It is in the ***atmospheric windows*** between absorption bands that practical earth space communications have developed, and it is in these windows that we will focus our attention in our study of transmission impairments.

6.2 Radiowave Propagation Mechanisms

Before beginning our detailed discussion of radiowave propagation in space communications, it will be useful to introduce the general terms used to describe the propagation phenomena, or ***propagation mechanisms***, which can affect the characteristics of a radiowave. The mechanisms are usually described in terms of variations in the signal characteristics of the wave, as compared to the natural or free space values found in the absence of the mechanism. The definitions presented here are meant to be general and introductory. Later chapters will discuss them in more detail. Most of the definitions are based on the Institute of Electrical and Electronics Engineers (IEEE) Standard Definitions of Terms for Radio Wave Propagation [2].

www.EngineeringBooksPdf.com

6.2.1 Absorption

A reduction in the amplitude (field strength) of a radiowave caused by an irreversible conversion of energy from the radiowave to matter in the propagation path.

6.2.2 Scattering

A process in which the energy of a radiowave is dispersed in direction due to interaction with inhomogeneities in the propagation medium.

6.2.3 Refraction

A change in the direction of propagation of a radiowave resulting from the spatial variation of refractive index of the medium.

6.2.4 Diffraction

A change in the direction of propagation of a radiowave resulting from the presence of an obstacle, a restricted aperture, or other object in the medium.

6.2.5 Multipath

The propagation condition that results in a transmitted radiowave reaching the receiving antenna by two or more propagation paths. Multipath can result from refractive index irregularities in the troposphere or ionosphere, or from structural and terrain scattering on the Earth's surface.

6.2.6 Scintillation

Rapid fluctuations of the amplitude and the phase of a radiowave caused by small-scale irregularities in the transmission path (or paths) with time.

6.2.7 Fading

The variation of the amplitude (field strength) of a radiowave caused by changes in the transmission path (or paths) with time. The terms fading and scintillation are often used interchangeably, however, fading is usually used to describe slower time variations, on the order of seconds or minutes, whereas scintillation refers to more rapid variations, on the order of fractions of a second in duration.

6.2.8 Frequency Dispersion

A change in the frequency and phase components across the bandwidth of a radiowave, caused by a dispersive medium. A dispersive medium is one whose constitutive components (permittivity, permeability, and conductivity) depend on frequency (temporal dispersion) or wave direction (spatial dispersion).[1]

Many of the mechanisms described above can be present on the transmission path at the same time and it is usually extremely difficult to identify the mechanism or

1 The term dispersion is also used to denote the differential delay experienced across the bandwidth of a radiowave propagating through a medium of free electrons, such as the ionosphere or a plasma field.

www.EngineeringBooksPdf.com

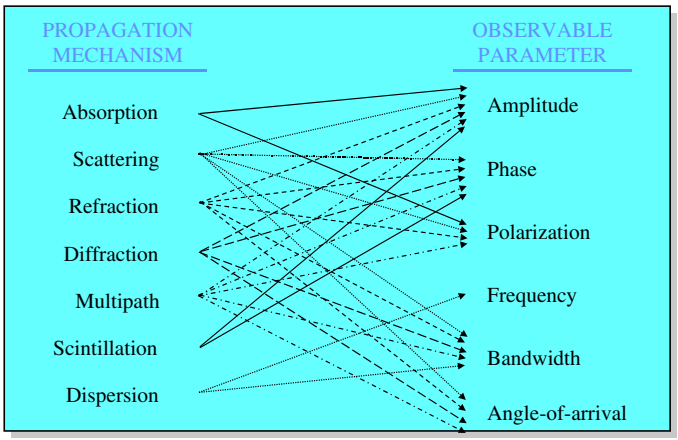

Figure 6.3 Radiowave propagation mechanisms and their impact on the parameters of a communications signal. (Source: Ippolito [1]; reproduced by permission of Van Nostrand Reinhold.)

mechanisms, which produce a change in the characteristics of the transmitted signal. This situation is illustrated in Figure 6.3, which indicates how the various propagation mechanisms affect the measurable parameters of a signal on a communications link. The parameters that can be observed or measured on a typical link are amplitude, phase, polarization, frequency, bandwidth, and angle of arrival. Each of the propagation mechanisms, if present in the path, will affect one or more of the signal parameters, as shown on the figure. Since all of the signal parameters, except for frequency, can be affected by several mechanisms, it is usually not possible to determine the propagation conditions from an observation of the parameters alone, For example, if a reduction in signal amplitude is observed, it could be caused by absorption, scattering, refraction, diffraction, multipath, scintillation, fading, or a combination of the above.

Propagation effects on communications links are usually defined in terms of variations in the signal parameters, hence one or several mechanisms could be present on the link. A reduction of signal amplitude caused by rain in the path, for example, is the result of both absorption and scattering. As we proceed through our discussion of propagation factors in this and succeeding chapters, it will be helpful to recall the differentiation between the propagation effect on a signal parameter and the propagation mechanisms which produce the variation in the parameter.

We have seen that frequency plays a major role in the determination of the propagation characteristics of radiowaves used for space telecommunications, and that the ionosphere is a critical element in the evaluation of propagation effects. It is useful, therefore, to divide the introductory discussion of transmission impairments found in space communications into two regions of the frequency spectrum: a lower frequency region where the effects are primarily produced in the ionosphere, and a higher frequency region where the effects are primarily produced in the troposphere, that is, where the ionosphere is essentially transparent to the radiowave, and a lower frequency region where the effects are determined by the ionosphere.

The breakpoint between the two regions is not at a specific frequency, but generally will occur at around 3 GHz (10 cm wavelength). There is some overlap for certain propagation conditions, and these will be discussed when appropriate. The following

www.EngineeringBooksPdf.com

two sections introduce the major propagation factors found in the two regions, which impact transmissions in the two frequency regions. Later chapters will discuss the factors in more detail and will emphasize their impact on communications link design and performance.

6.3 Propagation Below About 3 GHz

The major propagation impairments which can affect space communications at frequencies above the ionospheric penetration frequency and up to about 3 GHz are introduced in this section. Satellite communications applications which operate in the frequency bands below about 3 GHz include:

- user links for mobile satellite networks (land, aeronautical, and maritime),
- satellite cellular mobile user links
- command and telemetry links supporting satellite operations
- deep space communications, and
- specialized services where wide directivity ground antennas are important.

The ionosphere is the primary source of transmission impairments on satellite communications links operating in the frequency bands up to about 3 GHz. Two main characteristics of the ionosphere contribute to the degradation of radio waves:

(1) background ionization quantified by the ***total electron content*** (TEC) along the propagation path, and,
(2) ionospheric irregularities along the path.

The degradations related to TEC include Faraday rotation, group delay, dispersion, Doppler frequency shift, variation in direction of arrival, and absorption. The main effect attributed to ionospheric irregularities is scintillation. We first describe the basic characteristics of the ionosphere before introducing the propagation impairments, which can hinder space communications in the frequency bands below about 3 GHz.

The ionosphere is a region of ionized gas or plasma that extends from about 15 km to a not very well defined upper limit of about 400 km to 2000 km about the Earth's surface. The ionosphere is ionized by solar radiation in the ultraviolet and x-ray frequency range and contains free electrons and positive ions so as to be electrically neutral. Only a fraction of the molecules, ($< 1\%$ in the F layer) mainly oxygen and nitrogen, are ionized in the lower ionosphere, and large numbers of neutral molecules are also present. It is the free electrons that affect electromagnetic wave propagation for satellite communications.

Because different portions of the solar spectrum are absorbed at different altitudes, the ionosphere consists of several layers or regions of varying ion density. By increasing altitude, these layers are known as the D, E, and F layers, see Figure 6.1. The layers are not sharply defined since the transition from one to the other is generally gradual with no pronounced minimum in electron density in between. Representative plots of electron density are shown on Figure 6.4.

The density of electrons in the ionosphere also varies as a function of geomagnetic latitude, diurnal cycle, yearly cycle, and sunspot cycle (among others). Most temperate region ground-station-satellite paths pass through the mid-latitude electron-density region, which is the most homogeneous region. High latitude stations may be affected

www.EngineeringBooksPdf.com

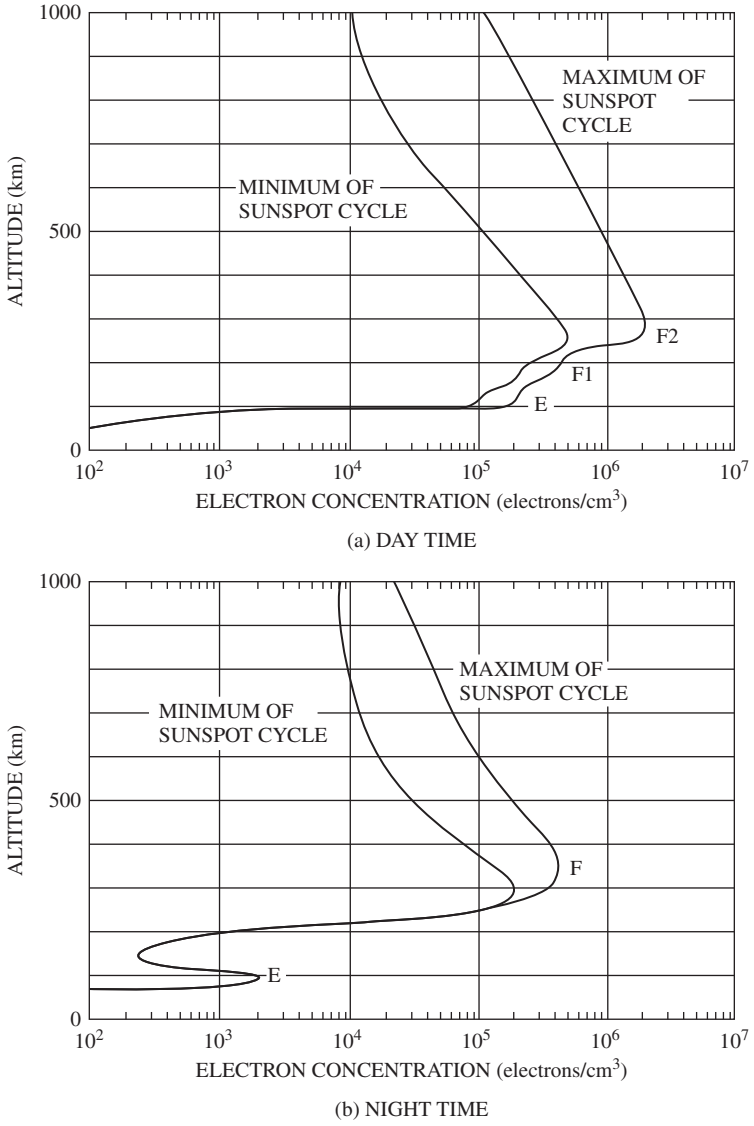

Figure 6.4 Examples of electron density distributions (from Hanson WB., "Structures of the Ionosphere" in Johnson, F.S. (ed.), Satellite Environment Handbook, Stanford University Press, 1965). (Source: Flock [4]. Reproduced by permission of NASA.)

by the auroral region electron densities which are normally more irregular. A discussion of latitude effects is included in ITU-R Recommendation P.531–12 [3].

A brief overview of the significant ionospheric layers D, E, and F, summarized from [4], is presented here.

The ***D layer***, the lowest of the ionospheric layers, extends from approximately 50 to 90 km with the maximum electron density of about $10^9/\text{m}^3$ occurring between 75 and 80 km in the daytime. At night, electron densities throughout the D layer drop to

www.EngineeringBooksPdf.com

small values. The D layer has little effect on radiowave scintillation since the electron concentration is low. However, attenuation in the ionosphere occurs mainly through collisions of electrons with neutral particles, and since the D layer is at a low altitude many neutral atoms and molecules are present and the collision frequency is high. Therefore transmissions in the AM broadcast band (0.5 MHz to 1.6 MHz) are highly attenuated in the day time D layer, but distant reception becomes possible at night when the D layer disappears.

The ***E layer*** extends from about 90 to 140 km, and the peak electron concentration occurs between about 100 and 110 km. Electron densities in the E layer vary with the 11-year sunspot cycle and are about $10^{11}/m^3$ at the minimum of the sunspot cycle and about 50% greater at the peak of the cycle. Electron concentrations drop by a factor of about 100 at night but there is always residual ionization. Intense electrical currents flow in the equatorial and auroral ionospheres at E layer altitudes (90 km to 140 km), these currents being known as ***equatorial and auroral electrojets***. Radio waves are scattered from electron-density structures associated with the electrojets at or slightly above 1 GHz. Backscatter echoes from the auroral electrojets indicate the regions of occurrence of auroras and are referred to as ***radio auroras***. The phenomena of sporadic E, thin sporadic, often discontinuous layers of intense ionization, occur in the E layer, at times with apparent electron densities well above $10^{12}/m^3$. The E layer is useful for communications, as HF (3-30 MHz) waves may be reflected from the E layer at frequencies that are a function of time of day and period of the sunspot cycle. By causing interference between VHF (30-300 MHz) stations, sporadic E tends to be a nuisance.

The ***F layer*** has the highest electron densities of the normal ionosphere. In the daytime it consists of two parts, the ***F1 and F2 layers***. The F1 layer largely disappears at night but has peak densities of about $1.5 \times 10^{11}/m^3$ at noon at the minimum of the sunspot cycle and $4 \times 10^{11}/m^3$ at noon at the peak of the sunspot cycle. The F2 layer has the highest peak electron densities of the normal ionosphere and the electron densities there remain higher at night than in the D and E regions. The peak electron density is in the 200 to 400 km height range and may be between about $5 \times 10^{11}/m^3$ and $4 \times 10^{11}/m^3$ at night, reaching a deep diurnal minimum near dawn. Daytime electron densities of about $5 \times 10^{12}/m^3$ have been measured in the F layer. Reflection from the F2 layer is the major factor in HF communications, which formerly handled a large fraction of long distance, especially transoceanic, communications.

The integrated or total electron content (TEC) along the ray path from transmitter to receiver is significant in determining ionospheric effects on communication signals. The TEC is defined as the number of electrons in a column one square meter in cross section (el/m^2) that coincides in position with the propagation path. The TEC for a propagation path s, is determined from integration of the electron concentration along the total path, that is [3],

$$N_T = \int_s n_e(s)\, ds \tag{6.1}$$

where:

N_T = the total electronic content (TEC), in el/m^2
s = the propagation path, in m
n_e = electron concentration, in el/m^3

www.EngineeringBooksPdf.com

The TEC of the ionosphere has a pronounced diurnal variation and also varies with solar activity, especially with geomagnetic storms that result from solar activity. It tends to peak during the sunlit portion of the day. Faraday rotation, excess time delay, and associated range delay, phase advance, and time delay and phase advance dispersion are directly proportional to TEC. Most ionospheric effects on radio propagation tend to be proportional to TEC.

Representative curves showing the diurnal variation of TEC are shown in Figure 6.5. The data were obtained at Sagamore Hill, MA, USA using 136 MHz signals from the NASA ATS-3 satellite.

The major impairments discussed here are; ionospheric scintillation, polarization rotation, group delay and dispersion. Other ionospheric effects, such as ionospheric absorption and angle of arrival variations, are generally of second order importance and will not adversely affect performance or systems design for satellite communications applications. Second order effects descriptions can be found in [3] and [4].

We focus here on ***line-of-site*** link impairments; additional effects, such as shadowing, blockage and multipath scintillation, which may be present on satellite links involving mobile terminals, are discussed in Chapter 12, Mobile Satellite Networks.

6.3.1 Ionospheric Scintillation

Ionospheric scintillation consists of rapid fluctuations of the amplitude and phase of a radiowave, caused by electron density irregularities in the ionosphere. Scintillation effects have been observed on links from 30 MHz to 7 GHz, with the bulk of observations of amplitude scintillation in the VHF (30 to 300 MHz) band [3]. The scintillation can be very severe and can determine the practical limitation for reliable communications under certain atmospheric conditions. Ionospheric scintillation is most severe for transmission through equatorial, auroral, and polar regions; and during sunrise and sunset periods of the day. The principal mechanisms of ionospheric scintillation are forward scattering and diffraction.

A ***scintillation index*** is used to quantify the intensity fluctuations of ionospheric scintillation. The most common scintillation index, denoted S_4, is defined as

$$S_4 = \left(\frac{\langle I^2 \rangle - \langle I \rangle^2}{\langle I \rangle^2} \right)^{\frac{1}{2}} \tag{6.2}$$

where I is the intensity of the signal, and $\langle\rangle$ denotes the average value of the variable.

The scintillation index is related to peak-to-peak fluctuations of the intensity. The exact relationship depends on the distribution of the intensity, but is well described by the Nakagami distribution for a wide range of S_4 values. As S_4 approaches 1.0, the distribution approaches the Rayleigh distribution. Under certain conditions wave focusing caused by the ionospheric irregularities can cause S_4 to exceed 1, reaching values as high as 1.5.

The scintillation index S_4 can be estimated from the peak-to-peak fluctuation, P_{p-p}, observed on a link from the approximate relationship

$$S_4 \cong 0.07197 \, {P_{p-p}}^{0.794} \tag{6.3}$$

where P_{p-p} is the peak-to-peak power fluctuation, in dB

This result, reported by the ITU [3], is based on empirical measurements of scintillation indices over a range of conditions. Note that a P_{p-p} of 10 dB corresponds to a

www.EngineeringBooksPdf.com

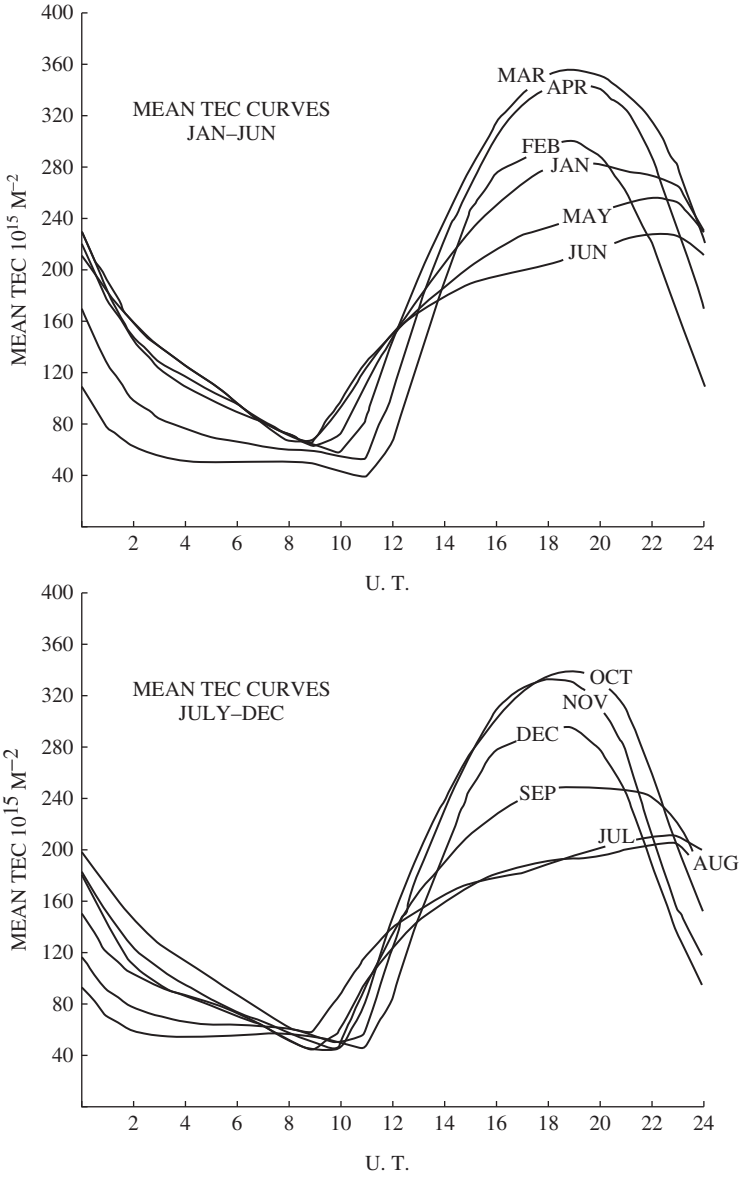

Figure 6.5 Diurnal variations in TEC, mean monthly curves for 1967 to 1973 as obtained at Sagamore Hill, MA, USA (after Hawkins & Klobuchar, 1974). (Source: Flock [4]; reproduced by permission of NASA.)

scintillation index of about 0.5, whereas a scintillation index of 1.0 results in a P_{p-p} of over 27 dB.

The two geographic areas with the most intense ionospheric scintillation are high latitude locations, and locations located near the magnetic equator. These areas are displayed on Figure 6.6, which shows areas of scintillation at L-band (1-2 GHz) for maximum and minimum solar activity conditions. The plot also shows the diurnal effect of

www.EngineeringBooksPdf.com

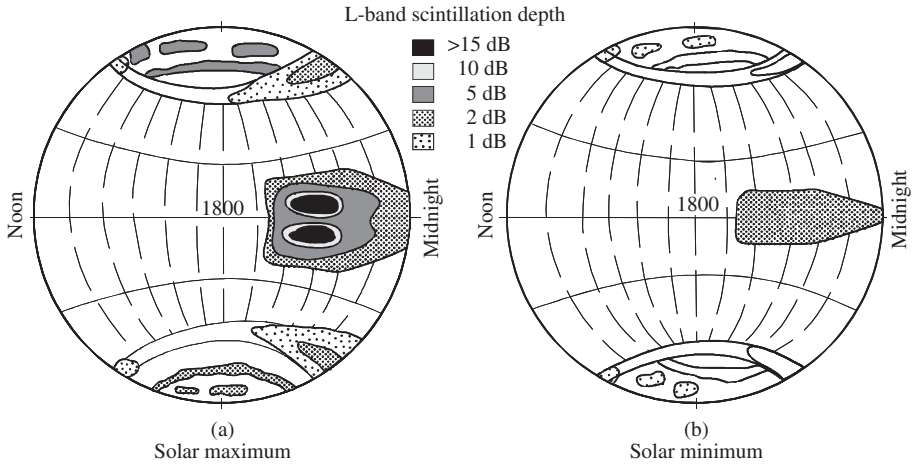

Figure 6.6 Regions of ionospheric scintillation. (Source: ITU-R [3]; reproduced by permission of International Telecommunications Union.)

the scintillation; the most intense zones occur near local midnight in a band within ±20° of the equator.

The fluctuation rate for ionospheric scintillation is fairly rapid, about 0.1 to 1 Hz. A typical scintillation event begins after local ionospheric sunset and can last from 30 minutes to several hours. Scintillation events occur almost every evening after sunset for equatorial locations in years of maximum solar activity. Peak-to-peak fluctuations of 10 dB and greater are not uncommon during these periods.

Ionospheric scintillation in the high latitude regions is generally not as severe as in the equatorial regions, rarely exceeding 10 dB, even during solar maximum conditions.

6.3.2 Polarization Rotation

Polarization rotation refers to a rotation of the polarization sense of a radiowave, caused by the interaction of a radiowave with electrons in the ionosphere, in the presence of the Earth's magnetic field. This condition, referred to as the ***Faraday Effect***, can seriously affect VHF space communications systems, which use linear polarization. A rotation of the plane of polarization occurs because the two rotating components of the wave progress through the ionosphere with different velocities of propagation.

The angle of rotation, θ, depends on the radiowave frequency, the magnetic field strength, and the electron density as

$$\theta = 236\ B_{av}\ N_T\ f^{-2} \tag{6.4}$$

where:

θ = angle of Faraday rotation, in rad
B_{av} = average Earth magnetic field, in Wb/m^2
f = radiowave frequency, in GHz
N_T = TEC, in el/m^2

Figure 6.7 shows the variation of Faraday rotation for frequencies from 100 MHz to 10 GHz, over a range of electron density from 10^{16} to 10^{19} el/m^2. A value of

www.EngineeringBooksPdf.com

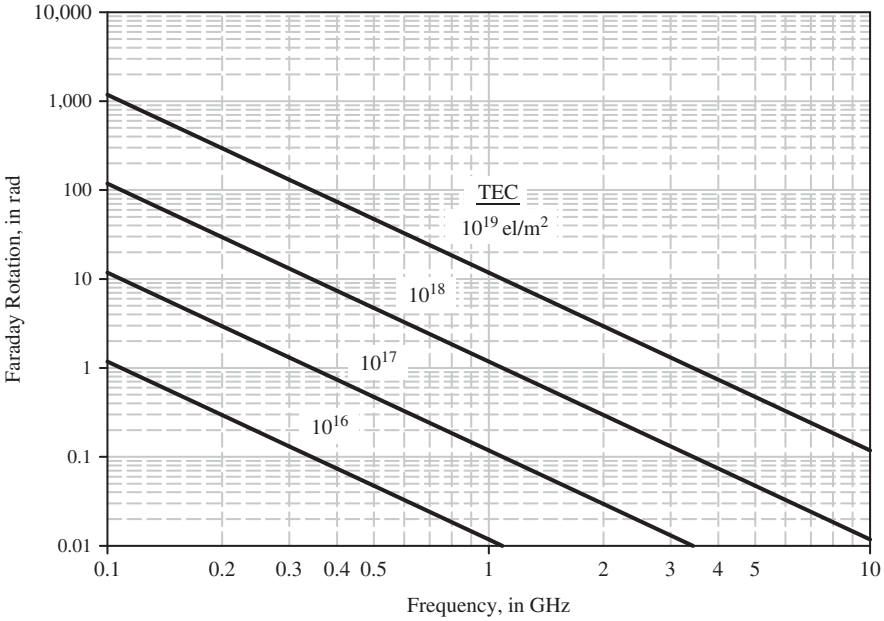

Figure 6.7 Faraday rotation angle as a function of operating frequency and TEC.

5×10^{-21} Wb/m^3 was assumed for the average magnetic field. Faraday rotation in the VHF/UHF region (300 MHz) can exceed 100 rad (15 full revolutions) for maximum TEC conditions, whereas the rotation at 3 GHz will be less about 1 radian for the same conditions.

Since Faraday rotation is directly proportional to the product of the electron density and the component of the Earth's magnetic field along the propagation path, its average value exhibits a very regular diurnal, seasonal, and solar cyclical behavior that is usually predictable. This allows the average rotation to be compensated for by a manual adjustment of the polarization tilt angle at the satellite earth-station antenna. However, large deviations from this regular behavior can occur for small percentages of the time as a result of geomagnetic storms and, to a lesser extent, large-scale travelling ionospheric disturbances. These deviations cannot be predicted in advance. Intense and fast fluctuations of the Faraday rotation angles at VHF have been associated with strong and fast amplitude scintillations respectively, at locations situated near the equator [3]. It should be emphasized again that Faraday rotation is a potential problem only for linearly polarized transmissions; circularly, polarized satellite links do not need to compensate.

6.3.3 Group Delay

Group delay (or propagation delay) refers to a reduction in the propagation velocity of a radiowave, caused by the presence of free electrons in the propagation path. The group velocity of a radiowave is retarded (slowed down), thereby increasing the travel time over that expected for a free space path. This effect can be extremely critical for radio navigation or satellite ranging links, which require an accurate knowledge of range and propagation time for successful performance.

www.EngineeringBooksPdf.com

Group delay is approximately proportional to the reciprocal of the frequency squared, and is of the form [3],

$$t = 1.345 \frac{N_T}{f^2} \times 10^{-25} \tag{6.5}$$

where

t = ionospheric group delay with respect to propagation in a vacuum, in s
f = radiowave frequency, in GHz
N_T = TEC, in el/m^2

Figure 6.8 shows the variation of ionospheric group delay over frequency for a range of electron density from 10^{16} to 10^{19} el/m^2. Delays of less than 1 μs are observed at L-band for the range of electron densities, while at VHF/UHF frequencies the delay can exceed 10 μs for maximum electron density conditions.

6.3.4 Dispersion

When a radiowave with a significant bandwidth propagates through the ionosphere, the propagation delay, which is a function of frequency, introduces ***dispersion***, the difference in the time delay between the lower and upper frequencies of the spectrum of the transmitted signal.

The differential delay across the bandwidth is proportional to the integrated electron density along the ray path [4]. For a fixed bandwidth the relative dispersion is inversely proportional to frequency cubed. The effect of dispersion is to introduce distortion into broadband signals, and systems at VHF and possibly UHF involving wideband transmissions must take this into account.

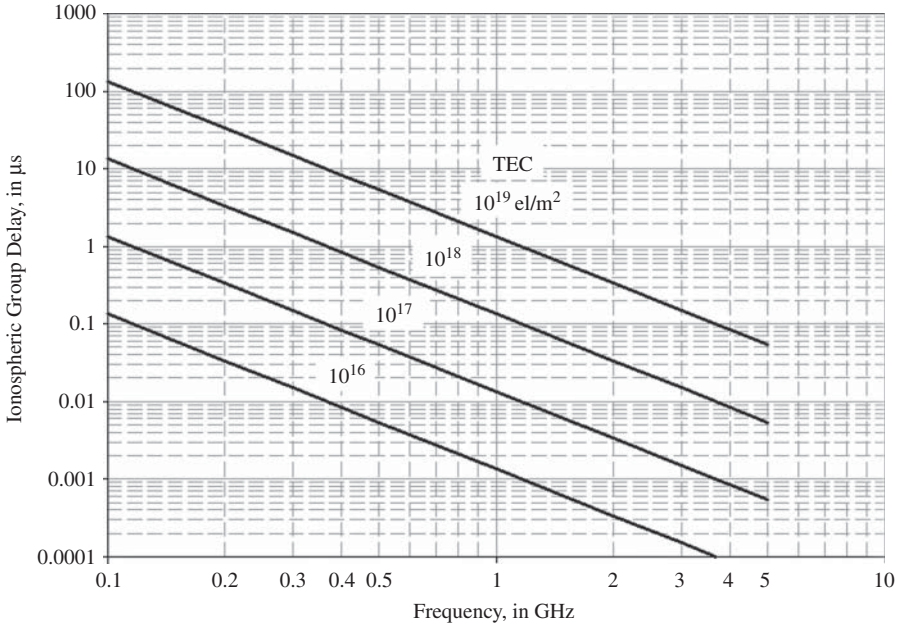

Figure 6.8 Ionospheric group delay as a function of operating frequency and TEC.

www.EngineeringBooksPdf.com

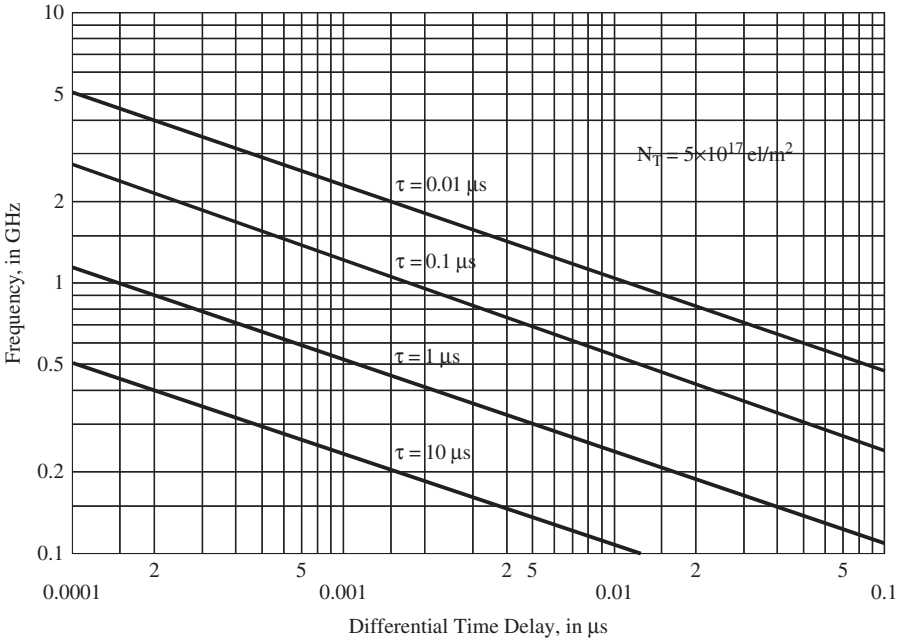

Figure 6.9 Dispersion for a pulse of width τ μs, transmitted through the ionosphere with a TEC level of 5×10^{17} el/m^2. (Source: ITU-R [3]; reproduced by permission of International Telecommunications Union.)

Figure 6.9 shows an ITU-R estimation of the differential time delay of a one-way transversal of the ionosphere with a TEC of 5×10^{17} el/m^2 [3]. The plot shows the difference in the time delay between the lower and upper frequencies of the spectrum of a pulse of width τ, transmitted through the ionosphere. The delay decreases with increasing frequency and decreasing pulse width. For example, a signal with a pulse length of 1 μs will sustain a differential delay of 0.02 μs at 200 MHz, whereas at 600 MHz the delay would be only 0.00074 μs.

The ***coherence bandwidth*** is defined as the upper limit on the information bandwidth or channel capacity that can be supported by a radiowave, caused by the dispersive properties of the atmosphere, or by multipath propagation. The coherence bandwidth caused by ionospheric dispersion is usually not a design factor, since the sustainable bandwidth far exceeds the bandwidth capabilities that the rf carrier can support. The coherence bandwidth due to all atmospheric causes for space communications frequencies up to 30 GHz and higher is one or more gigahertz, and is not generally a severe problem, except for very wideband (multi-gigabit) links and links, which must propagate through a plasma field, such as in space vehicle reentry.

6.4 Propagation Above About 3 GHz

The major propagation impairments, which can hinder space communications in the frequency bands above about 3 GHz are introduced and briefly described in this section. Many satellite communications links operate in the frequency bands above

www.EngineeringBooksPdf.com

3 GHz, including C-band, Ku-band, Ka-band, and V-band. Satellite applications which operate in these frequency bands include:

- fixed satellite service (FSS) user links
- broadcast satellite service (BSS) downlink user links
- BSS and mobile satellite service (MSS) feeder links
- deep space communications, and
- military communications links

The troposphere is the primary source of transmission impairments on satellite communications operating in these bands.

The impairments discussed here are rain attenuation, gaseous attenuation, cloud attenuation, rain and ice depolarization, and wet surface effects. We focus here on ***line-of-site*** link impairments; additional effects, such as shadowing, blockage, and multipath scintillation, which may be present on satellite links involving mobile terminals, are discussed in Chapter 12, Mobile Satellite Networks. The factors are presented in approximate order of decreasing impact to space communications system design and performance.

6.4.1 Rain Attenuation

Rain on the transmission path is the major weather effect of concern for earth-space communications operating in the frequency bands above 3 GHz. The rain problem is particularly significant for frequencies of operation above 10 GHz. Raindrops absorb and scatter radiowave energy, resulting in ***rain attenuation*** (a reduction in the transmitted signal amplitude), which can degrade the reliability and performance of the communications link. The non-spherical structure of raindrops also can change the polarization characteristics of the transmitted signal, resulting in ***rain depolarization*** (a transfer of energy from one polarization state to another). Rain effects are dependent on frequency, rain rate, drop size distribution, drop shape (oblateness) and, to a lesser extent, ambient temperature, and pressure.

The attenuating and depolarizing effects of the troposphere, and the statistical nature of these effects, are affected by macroscopic and microscopic characteristics of rain systems. The macroscopic characteristics include size, distribution, and movements of rain cells, the height of melting layers, and the presence of ice crystals. The microscopic characteristics include the size distribution, density, and oblateness of both raindrops and ice crystals. The combined effect of the characteristics on both scales leads to the cumulative distribution of attenuation and depolarization versus time, the duration of fades and depolarization periods, and the specific attenuation/depolarization versus frequency.

6.4.1.1 Spatial Structure of Rain

The relative impact of rain conditions on the transmitted signal depends on the spatial structure of rain. Two types of rain structure are important in the evaluation of rain effects on earth space communications; stratiform rain and convective rain.

6.4.1.1.1 Stratiform Rain In mid-latitude regions, stratiform rainfall is the type of rain, which typically shows stratified horizontal extents of hundreds of kilometers, duration times exceeding one hour and rain rates less than about 25 mm/h (1 inch/h). Stratiform rain usually occurs during the spring and fall months and, because of the cooler

www.EngineeringBooksPdf.com

temperatures, results in vertical heights of 4 to 6 km. For communications applications, stratiform rain represents a rain rate, which occurs for a sufficiently long period that a link margin may be required to exceed the attenuation associated with a one-inch per hour (25 mm/h) rain rate.

6.4.1.1.2 Convective Rain Convective rains arise from vertical atmospheric motions resulting in vertical transport and mixing. The convective flow occurs in a cell whose horizontal extent is usually several kilometers. The cell extends to heights greater than the average freezing layer at a given location because of convective upwelling. The cell may be isolated or embedded in a thunderstorm region associated with a passing weather front. Because of the motion of the front and the sliding motion of the cell along the front, the high rain rate duration is usually only several minutes in extent. These rains are the most common source of high rain rates in the U.S. and temperate regions of the world.

Stratiform rain covers large geographic locations and the spatial distribution of total rainfall from one of these storms is expected to be uniform. Likewise the rain rate averaged over several hours is expected to be rather similar for ground sites located up to tens of kilometers apart. Convective storms, however, are localized and tend to give rise to spatially non-uniform distributions of rainfall and rain rate for a given storm.

6.4.1.2 Classical Description for Rain Attenuation

The classical development for the determination of rain attenuation on a transmitted radiowave is based on three assumptions describing the nature of radiowave propagation and precipitation [1]:

1. The intensity of the wave *decays exponentially* as it propagates through the volume of rain.
2. The raindrops are assumed to be *spherical* water drops, which both scatter and absorb energy from the incident radiowave.
3. The contributions of each drop are *additive* and are *independent* of the other drops. This implies a "single scattering" of energy, however, the empirical results of the classical development do allow for some "multiple scattering" effects.

The attenuation of a radiowave propagating through a volume of rain of extent L in the direction of propagation can be expressed as

$$A = \int_0^L \alpha \, dx \tag{6.6}$$

where α is the specific attenuation of the rain volume, expressed in dB/km, and the integration is taken along the extent of the propagation path, from $x = 0$ to $x = L$.

Consider a plane wave with a transmitted power of p_t watts incident on a volume of uniformly distributed spherical water drops, all of radius r, extending over a length L in the direction of wave propagation, as shown in Figure 6.10. Under the assumption that the intensity of the wave decays exponentially as it propagates through the volume of rain, the received power, p_r, will be

$$p_r = p_t e^{-kL} \tag{6.7}$$

where k is the attenuation coefficient for the rain volume, expressed in units of reciprocal length.

www.EngineeringBooksPdf.com

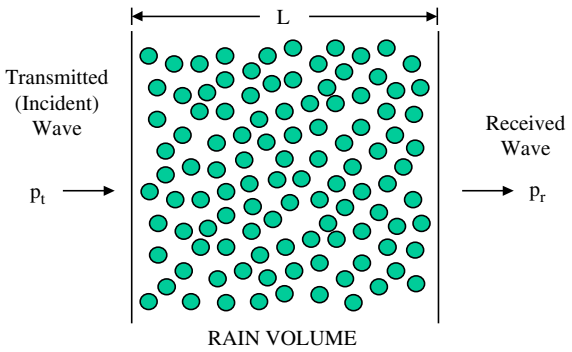

Figure 6.10 Plane wave incident on a volume of spherical uniformly distributed water drops. (Source: Ippolito [1]; reproduced by permission of Van Nostrand Reinhold.)

The attenuation of the wave, usually expressed as a positive decibel (dB) value, is given by

$$A(dB) = 10 \log_{10} \left(\frac{P_t}{P_r} \right) \tag{6.8}$$

Converting the logarithm to the base e and employing Eq. (6.7)

$$A(dB) = 4.343\, k\, L \tag{6.9}$$

The attenuation coefficient k is expressed as

$$k = \rho Q_t \tag{6.10}$$

where

ρ is the ***drop density***, that is, the number of drops per unit volume, and,
Q_t is the ***attenuation cross-section*** of the drop, expressed in units of area.

The cross-section describes the physical profile that an object projects to a radiowave. It is defined as the ratio of the total power extracted from the wave [watts] to the total incident power density [watts/(meter)^2], hence the units of area, (meter)^2.

For raindrops, Q_t is the sum of a scattering cross-section, Q_s, and an absorption cross-section, Q_a. The attenuation cross section is a function of the drop radius, r, wavelength of the radiowave, λ, and complex refractive index of the water drop, m. That is

$$Q_t = Q_s + Q_a = Q_t(r, \lambda, m) \tag{6.11}$$

The drops in a "real" rain are not all of uniform radius, and the attenuation coefficient must be determined by integrating over all of the drop sizes, that is,

$$k = \int Q_t(r, \lambda, m)\, \eta(r)\, dr \tag{6.12}$$

where $\eta(r)$ is the drop size distribution. $\eta(r)dr$ can be interpreted as the number of drops per unit volume with radii between r and r + dr.

The specific attenuation α, in dB/km, is found from Eqs. (6.9) and (6.12), with L = 1 km,

$$\alpha \left(\frac{dB}{km} \right) = 4.343 \int Q_t(r, \lambda, m)\, \eta(r)\, dr \tag{6.13}$$

www.EngineeringBooksPdf.com

The above result demonstrates the dependence of rain attenuation on drop size, drop size distribution, rain rate, and attenuation cross-section. The first three parameters are characteristics of the rain structure only. It is through the attenuation cross-section that the frequency and temperature dependence of rain attenuation is determined. All of the parameters exhibit time and spatial variability that are not deterministic or directly predictable, hence most analyses of rain attenuation must rely on statistical analyses to quantitatively evaluate the impact of rain on communications systems.

The solution of Eq. (6.13) requires Q_t and $\eta(r)$ as a function of the drop size, r.

Q_t can be found by employing the classical scattering theory of Mie for a plane wave radiating an absorbing sphere [6].

Several investigators have studied the distributions of raindrop size as a function of rain rate and type of storm activity, and the drop size distributions were found to be well represented by an exponential of the form

$$\eta(r) = N_0 e^{-\Lambda r} = N_0 e^{-[cR^{-d}]r} \tag{6.14}$$

where R is the rain rate, in mm/h, and r is the drop radius, in mm. N_0, Λ, c, and d are empirical constants determined from measured distributions [1].

The total rain attenuation for the path is then obtained by integrating the specific attenuation over the total path L, that is,

$$a(dB) = 4.343 \int_0^L \left[N_0 \int Q_t(r, \lambda, m)\, e^{-\Lambda r} dr \right] \, dl \tag{6.15}$$

where the integration over l is taken over the extent of the rain volume in the direction of propagation. Both Q_t and the drop size distribution will vary along the path and these variabilities must be included in the integration process. A determination of the variations along the propagation path is very difficult to obtain, particularly for slant paths to an orbiting satellite. These variations must be approximated or treated statistically for the development of useful rain attenuation prediction models.

6.4.1.3 Attenuation and Rain Rate

When measurements of rain attenuation on a terrestrial path were compared with the rain rate measured on the path, it was observed that the specific attenuation (dB/km) could be well approximated by

$$\alpha \left(\frac{dB}{km} \right) \cong a R^b \tag{6.16}$$

where R is the rain rate, in mm/h, and a and b are frequency and temperature dependent constants. The constants a and b represent the complex behavior of the complete representation of the specific attenuation as given by Eq. (6.13). This relatively simple expression for attenuation and rain rate was observed directly from measurements by early investigators such as Ryde & Ryde [7], and Gunn & East [8], however, analytical studies, most notably that of Olsen, Rogers & Hodge [9], have demonstrated an analytical basis for the aR^b expression. Appendix C of Ippolito [1] provides a full development of the analytical basis for the aR^b representation described above.

The use of the aR^b expression is included in virtually all current published models for the prediction of path attenuation from rain rate.

www.EngineeringBooksPdf.com

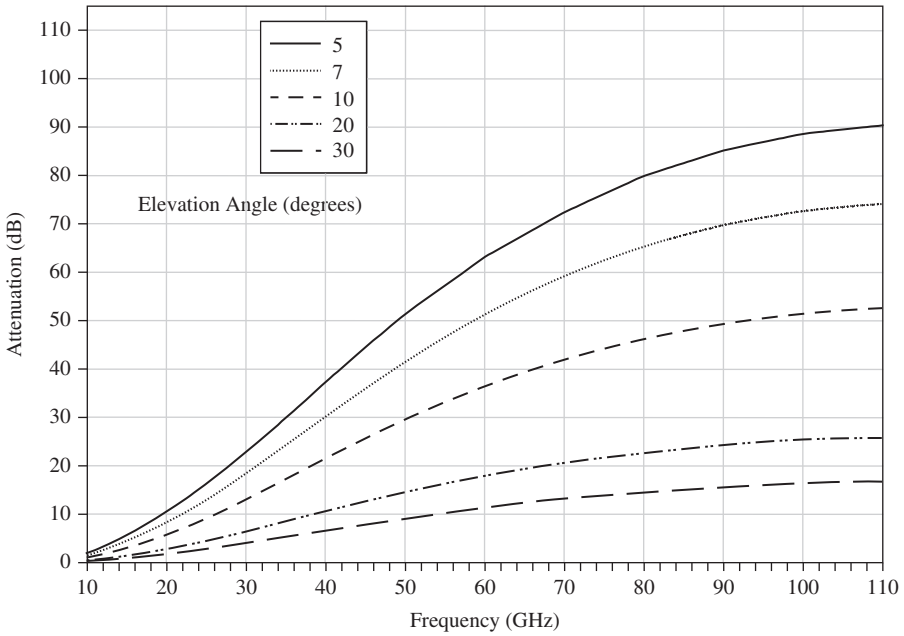

Figure 6.11 Total path rain attenuation as a function of frequency and elevation angle location: Washington, DC, link availability: 99%.

Figure 6.11 shows the rain attenuation expected for the worst 1% of an average year (which corresponds to a link availability of 99% for the year). The plots are for a ground terminal located in Washington, DC, and are shown for elevation angles to the satellite from 5 to 30 degrees.

Several general characteristics of rain attenuation are seen on the figure. Rain attenuation increases with increasing frequency, and with decreasing elevation angle. Rain attenuation levels can be very high, particularly for frequencies above 30 GHz. These plots are for a 99% annual link availability, which corresponds to a link outage (un-availability) of 1% or about 88 hours per year.

Models and procedures for the prediction of rain attenuation on satellite paths are presented in Chapter 7, Sec. 7.3.

6.4.2 Gaseous Attenuation

A radiowave propagating through the Earth's atmosphere will experience a reduction in signal level due to the gaseous components present in the transmission path. Signal degradation can be minor or severe, depending on frequency, temperature, pressure, and water vapor concentration. Atmospheric gases also affect radio communications by adding atmospheric noise (i.e., radio noise) to the link.

The principal interaction mechanism involving gaseous constituents and the radiowave is molecular absorption, which results in a reduction in signal amplitude (attenuation) of the signal. The absorption of the radiowave results from a quantum level change in the rotational energy of the molecule, and occurs at a specific resonant frequency or narrow band of frequencies. The resonant frequency of interaction

www.EngineeringBooksPdf.com

depends on the energy levels of the initial and final rotational energy states of the molecule.

The principal components of the atmosphere, and their approximate percentage by volume, are:

- oxygen (21%),
- nitrogen (78%),
- argon (0.9%), and
- carbon dioxide (0.1%),
- water vapor (variable, ~ 1.7% at sea level and 100% relative humidity)

Only **oxygen** and **water vapor** have observable resonance frequencies in the bands of interest, up to about 100 GHz, for space communications. Oxygen has a series of very close absorption lines near 60 GHz and an isolated absorption line at 118.74 GHz. Water vapor has lines at 22.3 GHz, 183.3 GHz, and 323.8 GHz. Oxygen absorption involves magnetic dipole changes, whereas water vapor absorption consists of electric dipole transitions between rotational states. Gaseous absorption is dependent on atmospheric conditions, most notably, air temperature and water vapor content.

Figure 6.12 shows the total gaseous attenuation observed on a satellite path located in Washington DC with elevation angles from 5 to 30 degrees. The values for the U.S. standard atmosphere, with an absolute humidity of 7.5 g/m^3 were assumed. The stark effect of the oxygen absorption lines at around 60 GHz is seen. The water vapor absorption line at 22.3 GHz is observed. As the elevation angle is decreased, the path length through the troposphere increases, and the resultant total attenuation increases. For

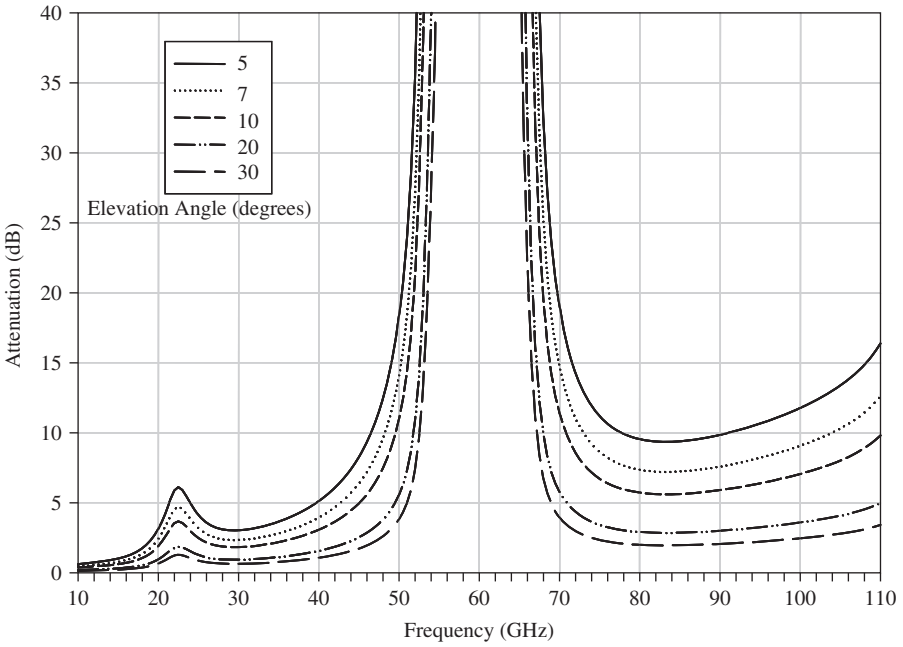

Figure 6.12 Total path gaseous attenuation versus frequency for elevation angles from 5 to 30 degrees, location: Washington DC.

www.EngineeringBooksPdf.com

Table 6.1 Observed characteristics of typical cloud types.

Cloud Type	Concentration (no/cm^3)	Liquid Water (g/m^3)	Average Radius *(microns)*
Fair-weather cumulus	300	0.15	4.9
Stratocumulus	350	0.16	4.8
Stratus (over land)	464	0.27	5.2
Altostratus	450	0.46	6.2
Stratus (over water)	260	0.49	7.6
Cumulus congestus	2-7	0.67	9.2
Cumulonimbus	72	0.98	14.8
Nimbostratus	330	0.99	9.0

(Source: Slobin [10]; reproduced by permission of American Geophysical Union.)

example, at 35 GHz, the path attenuation increases from about 0.7 dB to nearly 4 dB as the elevation angle decreases from 30 to 5 degrees.

Procedures for calculation of attenuation from atmospheric gases are presented in Chapter 7, Sec. 7.1.

6.4.3 Cloud and Fog Attenuation

Although rain is the most significant hydrometeor affecting radiowave propagation, the influence of clouds and fog can also be present on an earth-space path and must also be considered. Clouds and fog generally consist of water droplets of less than 0.1 mm in diameter, whereas raindrops typically range from 0.1 mm to 10 mm in diameter. Clouds are water droplets, not water vapor; however, the relative humidity is usually near 100% within the cloud. High-level clouds, such as cirrus, are composed of ice crystals, which do not contribute substantially to radiowave attenuation but can cause depolarization effects.

Attenuation due to fog is extremely low for frequencies less than about 100 GHz. The liquid water density in fog is typically about 0.05 g/m^3 for medium fog (visibility of the order of 300 m) and 0.5 g/m^3 for thick fog (visibility of the order of 50 m). Since the total path of a satellite link through the fog, even for low elevation angles, is short, on the order of 100s of meters, the total attenuation caused by fog can be neglected on consideration of links below 100 GHz. We will focus on the effects of clouds in the remainder of this section.

The average liquid water content of clouds varies widely, ranging from 0.05 to over 2 g/m^3. Peak values exceeding 5 g/m^3 have been observed in large cumulus clouds associated with thunderstorms; however, peak values for fair weather cumulus are generally less than 1 g/m^3. Table 6.1 summarizes the concentration, liquid water content, and droplet diameter for a range of typical cloud types (Slobin [10]).

6.4.3.1 Specific Attenuation for Clouds

The specific attenuation due to a cloud can be determined from:

$$\gamma_c = \kappa_c M \quad \text{dB/km} \tag{6.17}$$

www.EngineeringBooksPdf.com

where:

γ_c is the specific attenuation of the cloud, in dB/km,
κ_c is the specific attenuation coefficient, in (dB/km)/(g/m^3), and
M is the liquid water density in g/m^3.

The small size of cloud droplets allows the ***Rayleigh approximation*** to be employed in the calculation of specific attenuation. This approximation is valid for radiowave frequencies up to about 100 GHz. A mathematical model based on Rayleigh scattering, which uses a double-Debye model for the dielectric permittivity $\varepsilon(f)$ of water, can be used to calculate the value of κ_c for frequencies up to 1000 GHz:

$$\kappa_c = \frac{0.819f}{\varepsilon''(1+\eta^2)} \quad (\text{dB/km})/(\text{g/m}^3) \tag{6.18}$$

where f is the frequency in GHz, $\varepsilon'(f) + i\ \varepsilon''(f)$ is the complex dielectric permittivity of water and

$$\eta = \frac{2+\varepsilon'}{\varepsilon''} \tag{6.19}$$

Figure 6.13 shows the values of the specific attenuation K_c at frequencies from 5 to 200 GHz and temperatures between −8° C and 20° C.

6.4.3.2 Total Cloud Attenuation

The total attenuation due to clouds, A_T, can be determined from the statistics of

$$A_T = \frac{L\kappa_c}{\sin\theta} \quad \text{dB} \tag{6.20}$$

where:

θ = the elevation angle, ($5° \geq \theta \geq 90°$)
κ_c = the specific attenuation coefficient, in (dB/km)/(g/m^3), and
L = the total columnar content of liquid water, in kg/m^2 or, equivalently, in mm of precipitable water.

Statistics of the total columnar content of liquid water may be obtained from radiometric measurements or from radiosonde launches.

Figure 6.14 shows total cloud attenuation as a function of frequency, for elevation angles from 5 to 30 degrees (ITU-R) [11]. The calculations were based on stratus clouds with a cloud depth of 0.67 km, cloud bottom of 0.33 km, and a liquid water content of 0.29 g/m^3. The cloud attenuation is seen to increase with frequency and with decreasing elevation angle.

Procedures for the calculation of cloud attenuation are presented in Chapter 7, Sec. 7.2.

6.4.4 Depolarization

Depolarization refers to a change in the polarization characteristics of a radiowave caused by

a) hydrometeors, primarily rain or ice particles in the path, and
b) multipath propagation.

www.EngineeringBooksPdf.com

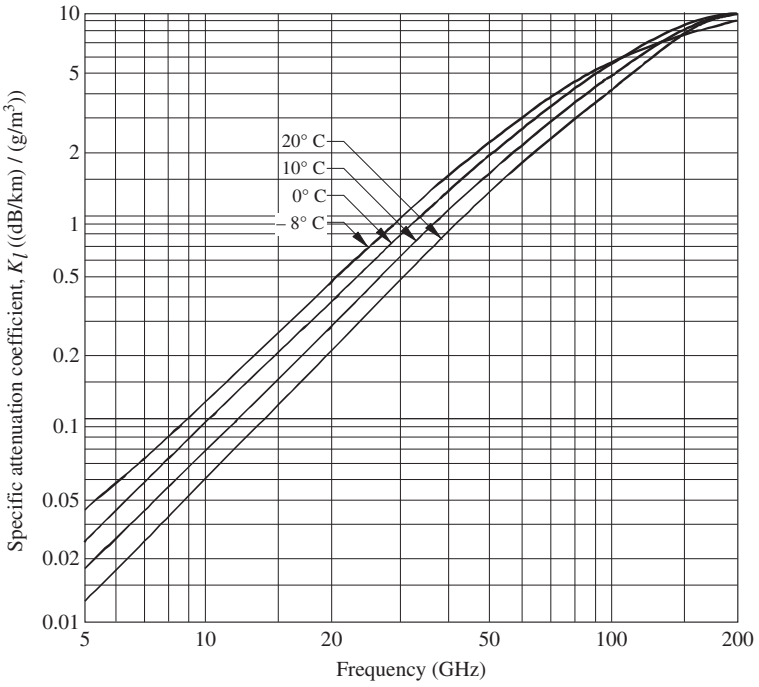

Figure 6.13 Specific attenuation for clouds as a function of frequency and temperature. (Source: ITU-R [11]; reproduced by permission of International Telecommunications Union.)

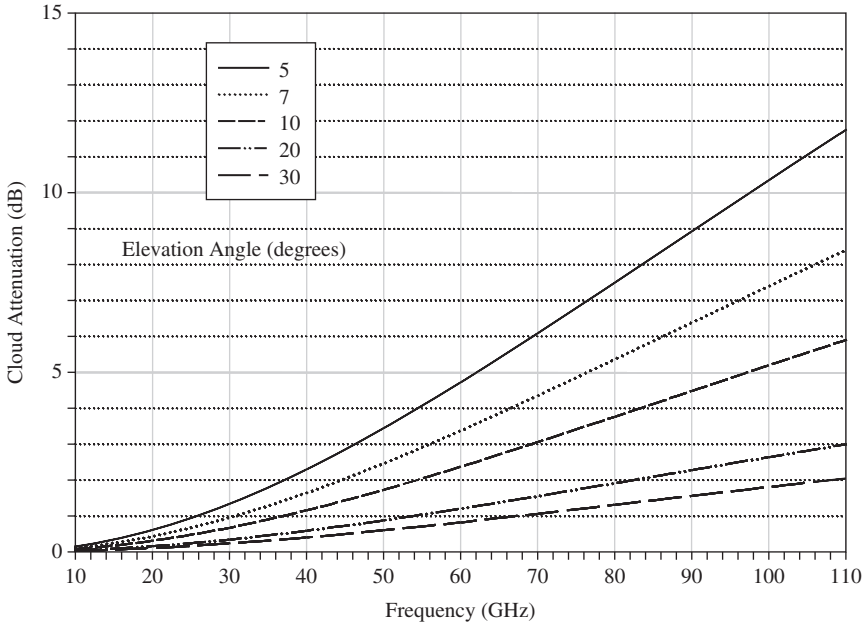

Figure 6.14 Total cloud attenuation as a function of frequency, for elevation angles from 5 to 30 degrees. (Source: ITU-R [11].)

www.EngineeringBooksPdf.com

A depolarized radiowave will have its polarization state altered such that power is transferred from the desired polarization state to an undesired orthogonally polarized state, resulting in interference or crosstalk between the two orthogonally polarized channels. Rain and ice depolarization can be a problem in the frequency bands above about 12 GHz, particularly for frequency reuse communications links, which employ dual independent orthogonal polarized channels in the same frequency band to increase channel capacity. Multipath depolarization is generally limited to very low elevation angle space communications, and will be dependent on the polarization characteristics of the receiving antenna.

6.4.4.1 Rain Depolarization

Rain induced depolarization is produced from a differential attenuation and phase shift caused by non-spherical raindrops. As the size of rain drops increase, their shape tends to change from spherical (the preferred shape because of surface tension forces) to oblate spheroids with an increasingly pronounced flat or concave base produced from aerodynamic forces acting upward on the drops. Furthermore, raindrops may also be inclined to the horizontal (canted) because of vertical wind gradients. The depolarization characteristics of a linearly polarized radiowave will depend significantly on the transmitted polarization angle.

An understanding of the depolarizing characteristics of the earth's atmosphere is particularly important in the design of ***frequency reuse communications systems*** employing dual independent orthogonal polarized channels in the same frequency band to increase channel capacity. Frequency reuse techniques, which employ either linear or circular polarized transmissions, can be impaired by the propagation path through a transferal of energy from one polarization state to the other orthogonal state, resulting in interference between the two channels.

Figure 6.15 shows a representation of the depolarization effect in terms of the E-field (electric field) vectors in a linearly polarized transmission link. The vectors E_1 and E_2 are the transmitted vertical and horizontal direction waves polarized 90 degrees apart (orthogonal) to provide two independent signals at transmission. The transmitted waves will be depolarized by the medium into several components, as shown on the right side of the figure.

The ***cross-polarization discrimination***, XPD, is defined for the linearly polarized waves as

$$XPD_1 = 20 \log \frac{|E_{11}|}{|E_{12}|} \tag{6.21}$$

for the linear vertical (1) direction, and

$$XPD_2 = 20 \log \frac{|E_{22}|}{|E_{21}|} \tag{6.22}$$

for the linear horizontal (2) direction.

E_{11} and E_{22} are the received electric field in the co-polarized (desired) 1 and 2 directions, respectively, and E_{12} and E_{21} are the electric fields converted to the orthogonal cross-polarized (undesired) directions 1 and 2.

A closely related parameter is the **isolation**, I, which compares the co-polarized received power with the cross-polarized power received in the same polarization state,

www.EngineeringBooksPdf.com

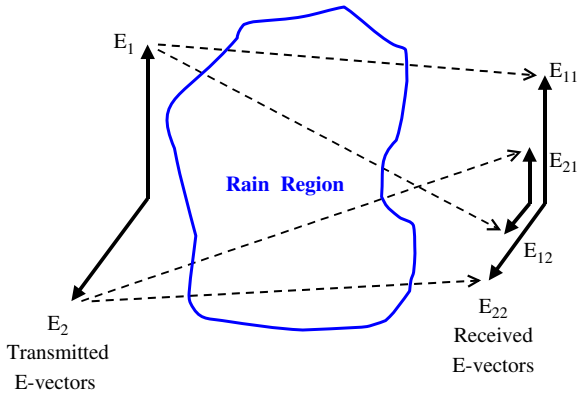

Figure 6.15 Depolarization components for linearly polarized waves.

that is,

$$I_1 = 20 \log \frac{|E_{11}|}{|E_{21}|} \tag{6.23}$$

for the vertical direction, and

$$I_2 = 20 \log \frac{|E_{22}|}{|E_{12}|} \tag{6.24}$$

for the horizontal direction.

Isolation takes into account the performance of the receiver antenna, feed and other components, as well as the propagating medium. When the receiver system polarization performance is close to ideal, then the XPD and I are nearly identical, and only the propagating medium contributes depolarizing effects to system performance.

The XPD and I for circular polarized transmitted waves can also be defined. The XPD for circular polarization can be shown to be nearly equivalent to the XPD for linear or horizontal polarized wave oriented at 45° from the horizontal [12].

The determination of the depolarization characteristics of rain requires knowledge of the ***canting angle*** of the raindrops, defined as the angle between the major axis of the drop and the local horizontal, shown as θ in Figure 6.16.

The canting angle for each raindrop in a typical rain will be different and will be constantly changing as it falls to the ground, since the aerodynamic forces will cause the drop to "wobble" and change orientation. Hence, for the modeling of rain depolarization a ***canting angle distribution*** is usually required and the XPD is defined in terms of the mean value of the canting angle. Measurements on earth-space paths using satellite beacons have shown that the average canting angle tends to be very close to 0 degrees

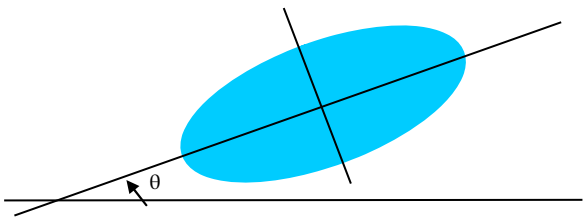

Figure 6.16 Canting angle for oblate spheroid rain drop.

www.EngineeringBooksPdf.com

(horizontal) for the majority of non-spherical raindrops [13]. Under this condition, the XPD for circular polarization is identical to the XPD for linear horizontal or vertical polarization oriented at 45 degrees from the horizontal.

When measurements of depolarization observed on a radiowave path were compared with rain attenuation measurements concurrently observed on the same path, it was noted that the relationship between the measured statistics of XPD and co-polarized attenuation, A, could be well approximated by the relationship

$$\text{XPD} = \text{U} - \text{V} \log \text{A} \qquad \text{(dB)} \tag{6.25}$$

where U and V are empirically determined coefficients which depend on frequency, polarization angle, elevation angle, canting angle, and other link parameters. This discovery is similar to the aR^b relationship observed between rain attenuation and rain rate discussed in Section 6.4.1.3. A theoretical basis for the relationship between rain depolarization and attenuation given above was developed by Nowland et al. [14], from small argument approximations applied to the scattering theory for an oblate spheroid raindrop.

For most rain depolarization prediction models, semi-empirical relations can be used for the U and V coefficients. An example of the application of a rain depolarization prediction model is shown in Figure 6.17. The figure shows cross polarization discrimination, XPD, as a function of frequency and elevation angle. The curves are for a ground terminal in Washington, DC, and the link availability was set at 99%.

Models and procedures for the prediction of rain depolarization are provided in Sec. 7.4.

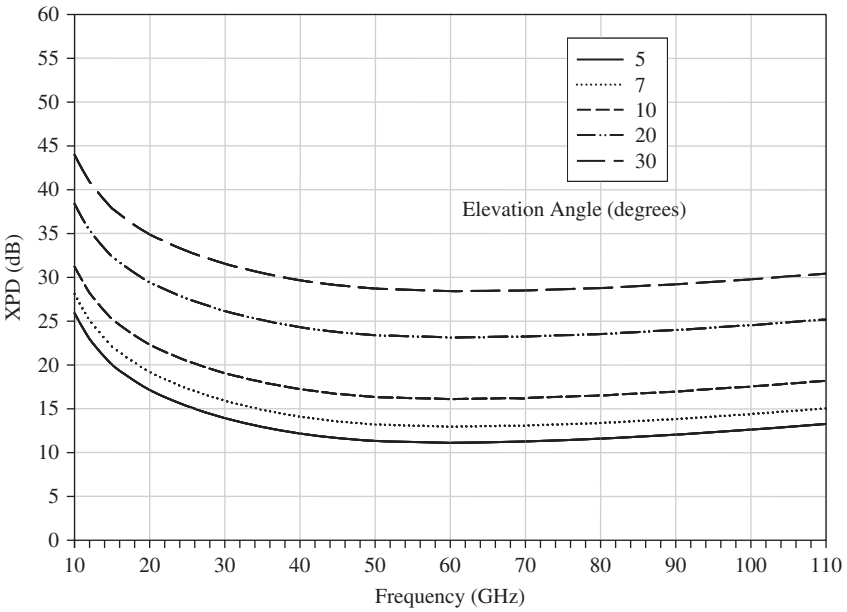

Figure 6.17 Rain depolarization XPD as a function of frequency and elevation angle location: Washington, DC, link availability: 99%.

www.EngineeringBooksPdf.com

6.4.4.2 Ice Depolarization

A second source of depolarization on an Earth-space path, in addition to rain, is the presence of ice crystals at high altitudes. Ice crystal depolarization is caused primarily by differential phase shifts rather than differential attenuation, which is the major mechanism for raindrop depolarization. Ice crystal depolarization can occur with little or no co-polarized attenuation. The amplitude and phase of the cross-polarized component can exhibit abrupt changes with large excursions.

Ice crystals form around dust particles in shapes influenced by the ambient temperature. In cirrus clouds they may exist for an indefinite time, but in cumulonimbus clouds they follow a cycle of growth by sublimation, falling and melting in the lower reaches of the cloud. Radio, radar, and optical observations confirm that cloud ice crystals possess some degree of preferred orientation related to the orientation of the electrostatic field. The crystals range in size from 0.1 to 1 mm and concentrations range from 10^3 to 10^6 crystals/m^3. The variation in concentration and occurrence of events may be due to the variation of "seed" nuclei in various air masses. For example, continental air masses contain more dust nuclei than maritime air masses and so occurrences of ice-crystal depolarization occur more frequently at inland ground stations.

Temperature and aerodynamic forces influence the shape of ice crystals. The two preferred shapes for ice crystals are *needles* and *plates*. At temperatures below −25°C the crystals are mainly needles, while for temperatures of −25°C to −9°C they are mainly plates. The crystals are very light and tend to fall very slowly [15] Ice depolarization effects have been observed on satellite links at frequencies from 4 GHz to 30 GHz and higher [1].

The contribution of ice depolarization to the total depolarization on a satellite link is difficult to determine from direct measurement, but can be inferred from observation of the copolarized attenuation during depolarization events. The depolarization, which occurs when the copolarized attenuation is low, (i.e., less than 1 to 1.5 dB), can be assumed to be caused by ice particles alone, whereas the depolarization that occurs when copolarized attenuation is higher can be attributed to both rain and ice particles.

The relative occurrence of ice depolarization versus rain depolarization is observed on Figure 6.18, which shows the three year cumulative distributions of XPD measured at Austin, Texas at 11.7 GHz [16]. The curve labeled RAIN + ICE is for all of the observed depolarization, whereas the RAIN ONLY curve corresponds to those measurements where the copolarized attenuation was greater than 1 dB. The ice contribution is observable only for XPD values greater than 25 dB, where ice effects are present about 10% of the time. The ice effects exceed 50% of the time at an XPD of 35 dB. The decrease in XPD caused by ice averages about 2 to 3 dB for a given percent of time.

Similar results were observed at 19 GHz from measurements reported at Crawford Hill, New Jersey, USA, using the COMSTAR beacons [17], summarized on Figure 6.19. For these measurements, ice depolarization was assumed for all times when the copolarized attenuation was 1.5 dB or less. Curves for RAIN + ICE, ICE ONLY, and RAIN ONLY, are shown. Again, the ice contribution is observable only for XPD values of 25 dB or greater, corresponding to an annual availability of about 0.063% for this data set. The decrease in XPD due to ice for a given time ranges from about 1 to 5 dB over that range.

Models and for the prediction of ice depolarization are provided in Sec. 7.4.

www.EngineeringBooksPdf.com

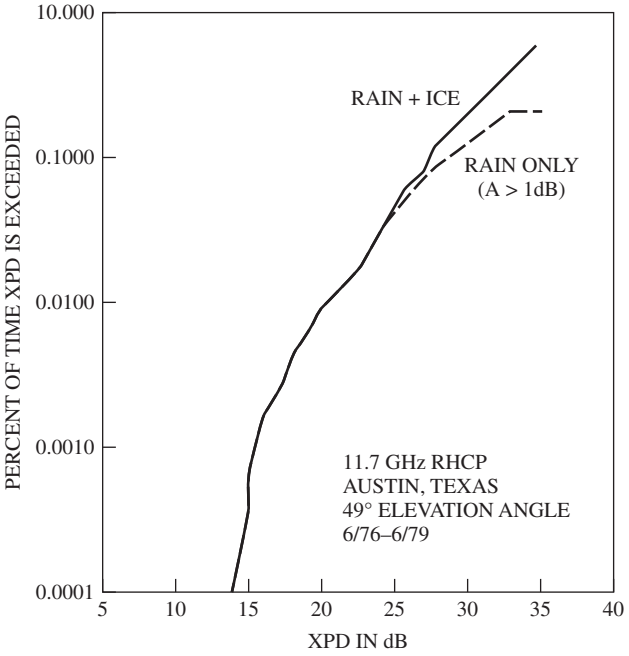

Figure 6.18 Rain and ice depolarization at 11.7 GHz. (Source: Ippolito [1]; reproduced by permission of Van Nostrand Reinhold.)

6.4.5 Tropospheric Scintillation

Scintillation describes the condition of rapid fluctuations of the signal parameters of a radiowave caused by time dependent irregularities in the transmission path. Signal parameters affected include:

- amplitude
- phase
- angle of arrival, and
- polarization.

Scintillation effects can be produced in both the ionosphere and in the troposphere. Electron density irregularities occurring in the ionosphere can affect frequencies up to about 6 GHz, whereas refractive index irregularities occurring in the troposphere cause scintillation effects in the frequency bands above about 3 GHz.

Tropospheric scintillation is produced by refractive index fluctuations in the first few kilometers of altitude and is caused by high humidity gradients and temperature inversion layers. The effects are seasonally dependent, vary day to day, and vary with the local climate. Tropospheric scintillation has been observed on line of site links up through 10 GHz and on earth space paths at frequencies to above 50 GHz.

To a first approximation, the refractive index structure in the troposphere can be considered horizontally stratified, and variations appear as thin layers that change with altitude. Slant paths at low elevation angles, that is, highly oblique to the layer structure, thus tend to be effected most significantly by scintillation conditions.

www.EngineeringBooksPdf.com

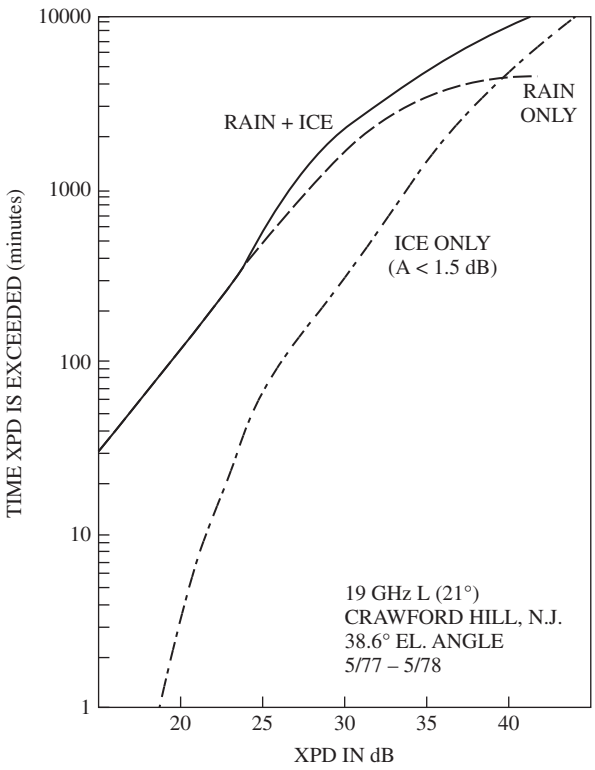

Figure 6.19 Rain and ice depolarization at 19 GHz. (Source: Ippolito [1]; reproduced by permission of Van Nostrand Reinhold.)

The general properties of the refractive index of the troposphere are well known. The atmospheric radio ***refractive index***, or index of refraction, n, at radiowave frequencies, is a function of temperature, pressure, and water vapor content. For convenience, since n is very close to 1, the refractive index properties are usually defined in terms of N units, or ***radio refractivity***, as

$$N = (n - 1) \times 10^6 = \frac{77.6}{T}\left(p + 4810\frac{e}{T}\right) \tag{6.26}$$

where:

p is the atmospheric pressure in millibars (mb),
e is the water vapor pressure in mb, and
T is the temperature, in degrees K.

The first term in Eq. (6.26) is often referred to as the "dry term"

$$N_{dry} = 77.6\frac{P}{T} \tag{6.27}$$

and the second term as the "wet term"

$$N_{wet} = 3.732 \times 10^5 \frac{e}{T^2} \tag{6.28}$$

This expression is accurate to within 0.5% for frequencies up to 100 GHz.

The long-term mean dependence of refractivity on altitude is found to be well represented by an exponential of the form,

$$N = 315\ e^{-\frac{h}{7.36}} \tag{6.29}$$

www.EngineeringBooksPdf.com

where h is the altitude, in km. This approximation is valid for altitudes up to about 15 km [18].

Small-scale variations of refractivity, such as those caused by temperature inversions or turbulence, will produce scintillation effects on a satellite signal. Quantitative estimates of the level of amplitude scintillation produced by a turbulent layer in the troposphere are determined by assuming small fluctuations on a thin turbulent layer and applying turbulence theory considerations of Tatarski [19].

6.4.5.1 Scintillation Parameters

Several parameters are used interchangeably in the literature to describe scintillation on a transmitted electromagnetic wave. In radiowave applications the received power or amplitude is of interest, whereas for optical wavelengths, intensity is typically measured. Other parameters include correlation functions and spectral representations to describe both turbulence and scintillation We will focus on the description of scintillation in terms of the received power of the transmitted wave, since we are interested in radiowave frequencies.

The log of the received power, expressed in dB, is defined as

$$x_{dB} = 20\log_{10}\left(\frac{A}{A_0}\right) \quad (dB) \tag{6.30}$$

where A is the received signal amplitude and $A_0 = \langle A \rangle$ is the average received amplitude.

In communication system applications, scintillation strength is often specified by the ***variance of the log of the received power***, σ^2_x, found in terms of the transmission parameters as

$$\sigma_x^2 = 42.25\ \left(\frac{2\pi}{\lambda}\right)^{7/6} \int_0^L C_n^2(x)\ x^{5/6}\ dx \tag{6.31}$$

where

C^2_n is the ***refractive index structure constant***,
λ is the wavelength,
x is the distance along the path, and
L is the total path length.

A precise knowledge of the amplitude scintillation depends on C^2_n, which is not easily available.

Eq. (6.31) shows that the r.m.s. amplitude fluctuation, σ_x, varies as $f^{7/12}$. Measurements at 10 GHz, which show a range of fluctuations from 0.1 to 1 dB, for example, would scale at 100 GHz to a range of about 0.38 to 3.8 dB.

6.4.5.2 Amplitude Scintillation Measurements

The most dominant form of scintillation observed on earth-space communications links involves the amplitude of the transmitted signal. Scintillation increases as the elevation angle decreases, since the path interaction region increases. Scintillation effects increase dramatically as the elevation angle drops below 10 degrees.

Scintillation measurements at frequencies from 2 GHz to above 30 GHz show broad agreement in general characteristics for scintillation at high elevation angles (20 to 30 degrees). In temperate climates the scintillation is on the order of 1 dB peak-to-peak in clear sky in the summer, 0.2 to 0.3 dB in winter, and 2 to 6 dB in cloud conditions.

www.EngineeringBooksPdf.com

Scintillation fluctuations vary over a large range, however, with fluctuations from 0.5 Hz to over 10 Hz. A much slower fluctuation component, with a period of one to three minutes, is often observed along with the more rapid scintillation discussed above. At low elevation angles, (below about 10 degrees), scintillation increased drastically, with less uniformity in structure and predictability. Deep fluctuations of 20 dB or more are observed, with durations of a few seconds in extent.

Figure 6.20 shows an example of low elevation amplitude scintillation measurements at 2 and 30 GHz made with the ATS-6 satellite at Columbus, Ohio, reported by Devasirvathm and Hodge [20]. The elevation angles to the satellite were 4.95 degrees (a), and 0.38 degrees (b). Measurements of this type were made in clear weather conditions up to an elevation angle of 44 degrees, and the data are summarized in Figure 6.21, where the mean amplitude variance is plotted as a function of elevation angle. The curves on the figure represent the minimum r.m.s. error fits to the assumed cosecant power law relation,

$$\sigma_x^2 \approx A(\csc\theta)^B \tag{6.32}$$

where θ is the elevation angle. The resulting B coefficients, as shown on the figure, compare well within their range of error with the expected theoretical value of 1.833 for a Kolmogorov type turbulent atmosphere.

Similar measurements were taken at 19 GHz with the COMSTAR satellites at Holmdel, NJ, USA (Titus & Arnold) [21]. Both horizontal and vertical polarized signals were monitored, at elevation angles from 1 to 10 degrees. Amplitude scintillation at the two polarization senses were found to be highly correlated, leading the authors to conclude that amplitude scintillation is independent of polarization sense.

Methods for the prediction of tropospheric scintillation on satellite paths are discussed in Sec. 7.5.

6.5 Radio Noise

Radio noise can be introduced into the transmission path of a satellite communications system from both natural and human-induced sources. Any natural absorbing medium in the atmosphere which interacts with the transmitted radiowave will not only produce a signal amplitude reduction (attenuation), but will also be a source of thermal noise power radiation. The noise associated with these sources, referred to as ***radio noise***, or ***sky noise***, will directly add to the system noise through an increase in the antenna temperature of the receiver. For very low noise communications receivers, radio noise can be the limiting factor in the design and performance of the system.

Radio noise is emitted from many sources, both natural (terrestrial and extra-terrestrial origin) and human made.

Terrestrial sources include:

- emissions from atmospheric gases (oxygen and water vapor)
- emissions from hydrometeors (rain and clouds).
- radiation from lightning discharges (atmospheric noise due to lightning);
- re-radiation from the ground or other obstructions within the antenna beam

www.EngineeringBooksPdf.com

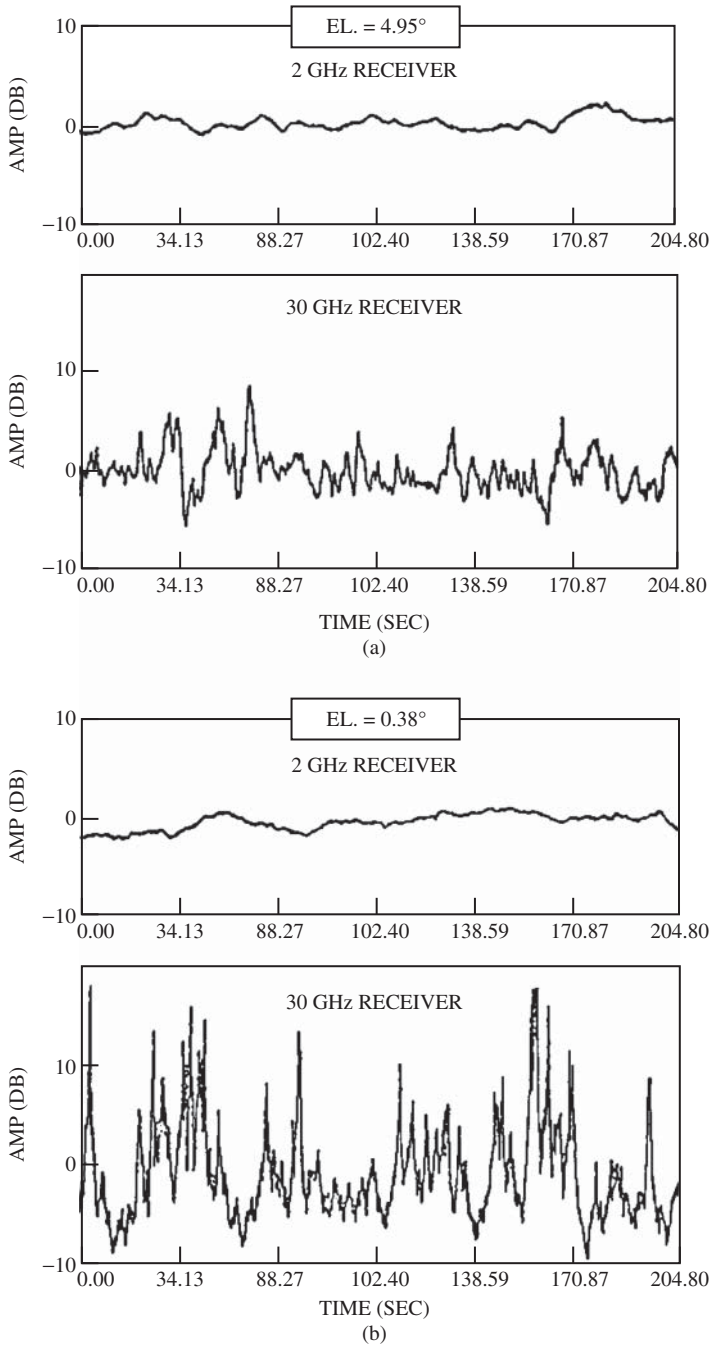

Figure 6.20 Scintillation on a satellite link for low elevation angles. (Source: Ippolito [1]; reproduced by permission of Van Nostrand Reinhold.)

www.EngineeringBooksPdf.com

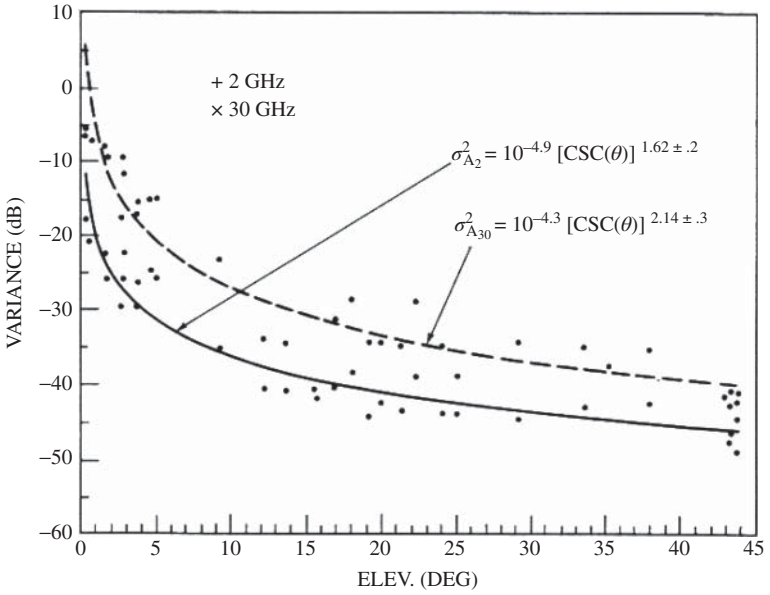

Figure 6.21 Mean amplitude variance for clear weather conditions, at 2 and 30 GHz, as a function of elevation angle. (Source: Ippolito [1]; reproduced by permission of Van Nostrand Reinhold.)

Extra-terrestrial sources include:

- cosmic background radiation
- solar and lunar radiation
- radiation from celestial radio sources (radio stars)

Human induced sources include:

- unintended radiation from electrical machinery, electrical and electronic equipment
- power transmission lines
- internal combustion engine ignition
- emission from other communications systems.

The following sections describe the major radio noise sources in satellite communications, and provide concise methods for the calculation radio noise for the evaluation of communications system performance.

6.5.1 Specification of Radio Noise

The thermal noise emission from a gas in thermodynamic equilibrium, from Kirchoff's Law, is equal to its absorption, and this equality holds for all frequencies. The noise temperature, t_b, observed by a ground station in a given direction through the atmosphere (also referred to as the brightness temperature), is given by radiative transfer theory, (Waters, 1976 [22]; Wulfsberg, 1964 [23]).

$$t_b = \int_0^\infty t_m \gamma e^{-\tau} dl + t_\infty e^{-\tau_\infty} \tag{6.33}$$

www.EngineeringBooksPdf.com

where t_m is the ambient temperature, γ is the absorption coefficient, and τ is the optical depth to the point under consideration. Also,

$$\tau = 4.343A \text{ dB} \tag{6.34}$$

where A is the absorption over the path in question, in dB. For frequencies above 10 GHz, the second term on the righthand side of Eq. (6.33) reduces to 2.7 K, the cosmic background component (unless the sun is in the beam of the aperture).

For an isothermal atmosphere (t_m constant with height), Eq. (6.33) further reduces to

$$t_b = t_m(1 - e^{\tau})$$

$$t_b = t_m\left(1 - 10^{-\frac{A}{10}}\right) \text{ K} \tag{6.35}$$

where A is again atmospheric absorption in dB. The value of t_m in Eq. (6.35) ranges from 260 to 280 K. Wulfsburg[34] provided a relationship to determine the value of t_m from surface measured temperature,

$$t_m = 1.12t_s - 50 \text{ K} \tag{6.36}$$

where t_s is the surface temperature, in K.

Noise from individual sources such as atmospheric gases, the Sun, the Earth's surface, and so on, are usually given in terms of their brightness temperature. The antenna temperature is the convolution of the antenna pattern and the brightness temperature of the sky and ground. For antennas whose patterns encompass a single distributed source, the antenna temperature and brightness temperature are the same.

The noise in a communications system is expressed in terms of an ***equivalent noise temperature***, t_a , in degrees Kelvin, and a noise factor, F_a , in dB, given by

$$F_a(\text{dB}) = 10\log\left(\frac{t_a}{t_0}\right) \tag{6.37}$$

where t_0 is the ambient reference temperature, set to 290 K. Equivalently, the ***noise factor*** can be expressed as

$$F_a\,(\text{dB}) = 10\log\left(\frac{p_a}{kt_0b}\right) \tag{6.38}$$

where p_a is the available noise power at the antenna terminals, k is Boltzman's constant, and b is the noise power bandwidth of the receiving system.

Figure 6.22, developed by the ITU-R (ITU-R P.372-12) [5], summarizes the median expected noise levels produced by sources of external radio noise in the frequency range applicable to practical space communications. Noise levels are expressed in terms of both noise temperature, t_a, (right vertical axis), and Noise Factor, F_a (dB) (left vertical axis). Between about 30 MHz to 1 GHz, galactic noise (curves B and C) dominates, but will generally be exceeded by man-made noise in populated areas (curve A). Above 1 GHz, the absorptive constituents of the atmosphere, that is, oxygen, water vapor (curves E), also act as noise sources and can reach a maximum value of 290 K under extreme conditions.

The sun is a strong variable noise source, reaching values of 10,000 K and higher when observed with a narrow beamwidth antenna (curve D), under quiet sun conditions. The cosmic background noise level of 2.7 K (curve F) is very low and is not a factor of concern in space communications.

www.EngineeringBooksPdf.com

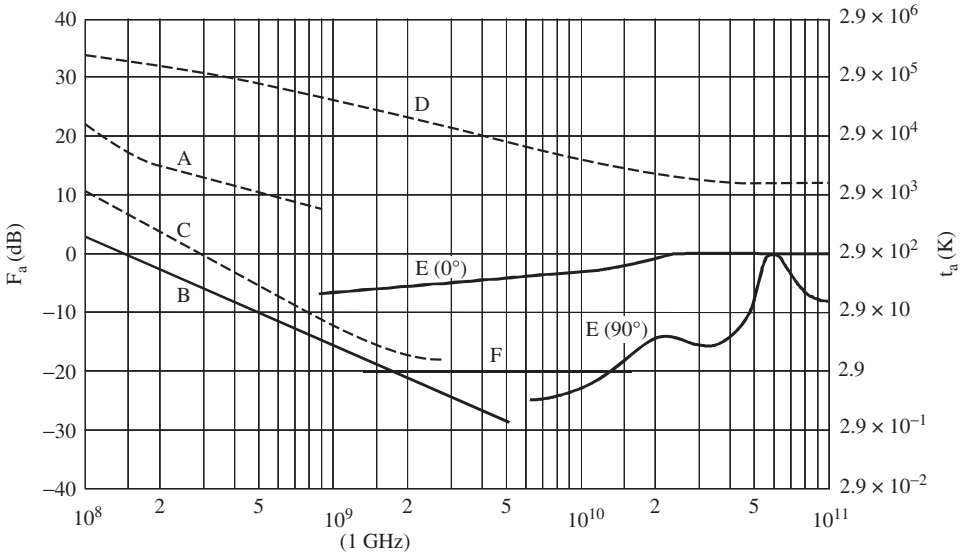

A: estimated median business area man-made noise
B: galactic noise
C: galactic noise (toward galactic centre with infinitely narrow beamwidth)
D: quiet Sun ($\frac{1}{2}^\circ$ beamwidth directed at Sun)
E: sky noise due to oxygen and water vapour (very narrow beam antenna); upper curve, 0° elevation angle; lower curve, 90° elevation angle
F: black body (cosmic background), 2.7 K minimum noise level expected

Figure 6.22 Noise factor and brightness temperature from external sources. (Source: ITU-R [5]; reproduced by permission of International Telecommunications Union.)

6.5.2 Noise From Atmospheric Gases

The gaseous constituents of the Earth's atmosphere interact with a radiowave through a molecular absorption process that results in attenuation of the signal. This same absorption process will produce a thermal noise power radiation that is dependent on the intensity of the absorption, through Eq. (6.35).

The major atmospheric gases that affect space communications are oxygen and water vapor. The sky noise temperature for oxygen and water vapor, for an infinitely narrow beam, at various elevation angles, was calculated by direct application of the radiative transfer equation, at frequencies between 1 and 340 GHz (Smith, 1982) [24]. Figures 6.23 and 6.24 summarize the results of these calculations for representative atmospheric conditions (ITU-R Rec. P.372-12) [5]. The two figures represent moderate atmospheric conditions (7.5 g/m^3 water vapor, 50% relative humidity). Figure 6.24 provides an expanded frequency scale version for use with frequencies below 60 GHz. The curves are calculated using a radiative transfer program for seven different elevation angles and an average atmosphere as stated on the figures. The cosmic noise contribution of 2.7 K or other extraterrestrial sources are not included. The 1976 United States Standard Atmosphere is used for the dry atmosphere. A typical water vapor contribution is added above the tropopause.

www.EngineeringBooksPdf.com

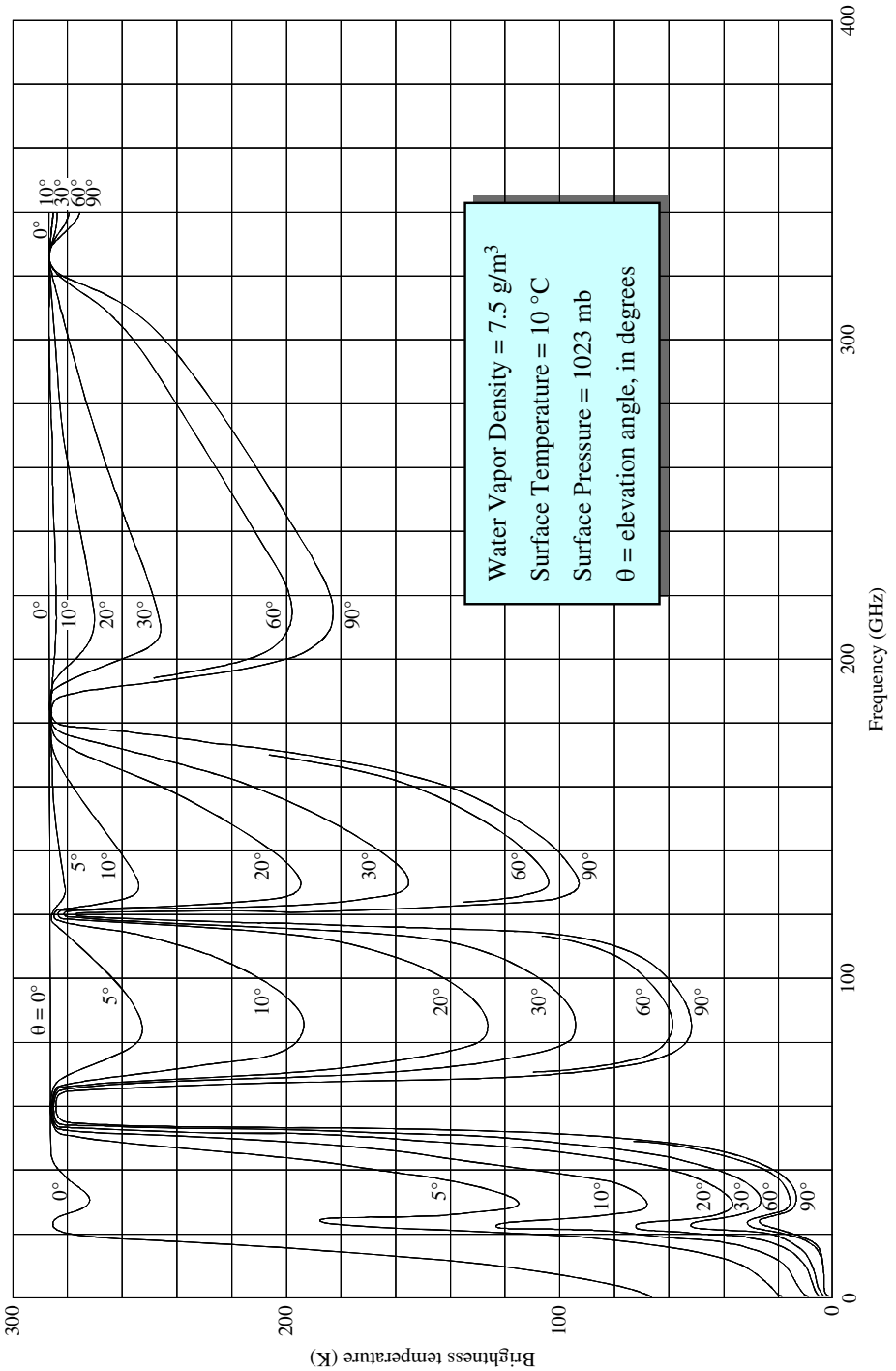

Figure 6.23 Brightness temperature of the atmosphere for moderate clear sky conditions. (Source: ITU-R [5]; reproduced by permission of International Telecommunications Union.)

www.EngineeringBooksPdf.com

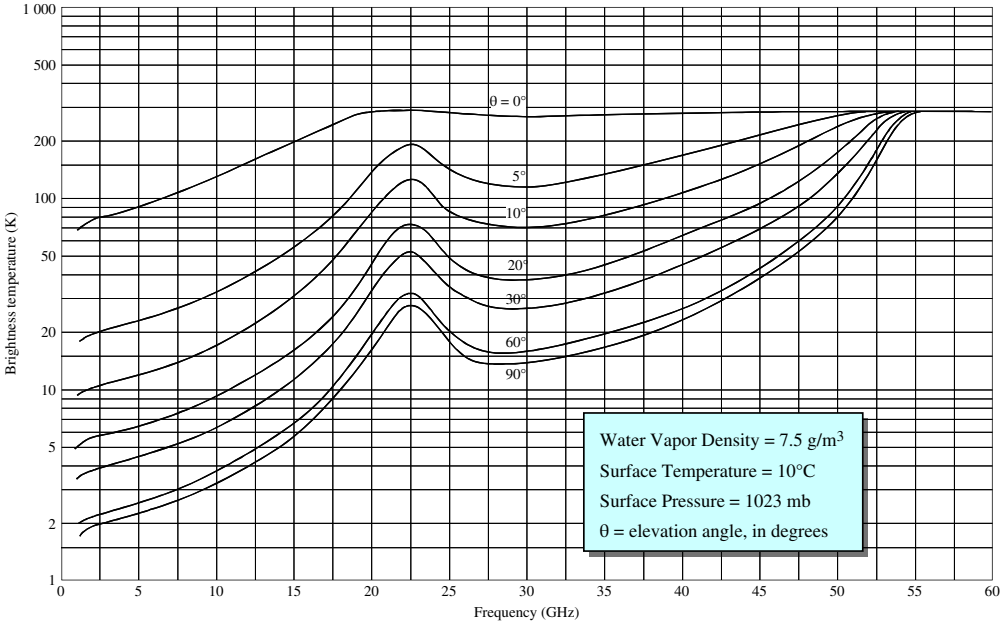

Figure 6.24 Brightness temperature of the atmosphere for moderate clear sky conditions – expanded scale; 1 to 60 GHz. (Source: ITU-R [5]; reproduced by permission of International Telecommunications Union.)

www.EngineeringBooksPdf.com

6.5.3 Sky Noise Due To Rain

Sky noise due to absorption in rain can also be determined from the radiative transfer approximation methods described in Sec. 5.9.1. The noise temperature due to rain, t_r, can be determined directly from the rain attenuation from (see Eq. (6.35))

$$t_r = t_m \left(1 - 10^{-\frac{A_r(dB)}{10}}\right) \qquad K \tag{6.39}$$

where t_m is the mean path temperature, in °K, and $A_r(dB)$ is the total path rain attenuation, in dB. Note that the noise temperature is independent of frequency, that is, for a given rain attenuation, the noise temperature produced will be the same, regardless of the frequency of transmission.

The mean path temperature, t_m, as described in Sec. 6.5.1, can be estimated from the surface temperature t_s by,

$$t_m = 1.12t_s - 50K \tag{6.40}$$

where t_s is the surface temperature in °K.

A direct measurement of t_m is difficult to obtain. Simultaneous measurements of rain attenuation and noise temperature on a slant path using satellite propagation beacons can provide a good estimate of the statistical range of t_m. Good overall statistical correlation of the noise temperature and attenuation measurements occurs for t_m between 270 K and 280 K for the vast majority of the reported measurements (Ippolito, 1971 [25]), (Strickland, 1974 [26]), (Hogg & Chu, 1975 [27]).

Figure 6.25 shows the noise temperature calculated from Eq. (6.39) as a function of total path rain attenuation for the range of values of t_m from 270 K to 280 K. The noise temperature approaches "saturation," that is, the value of t_m, fairly quickly above attenuation values of about 10 dB. Below that value the selection of t_m is not very critical. The centerline ($t_m = 275$ K) serves as the best prediction curve for t_r. The noise temperature

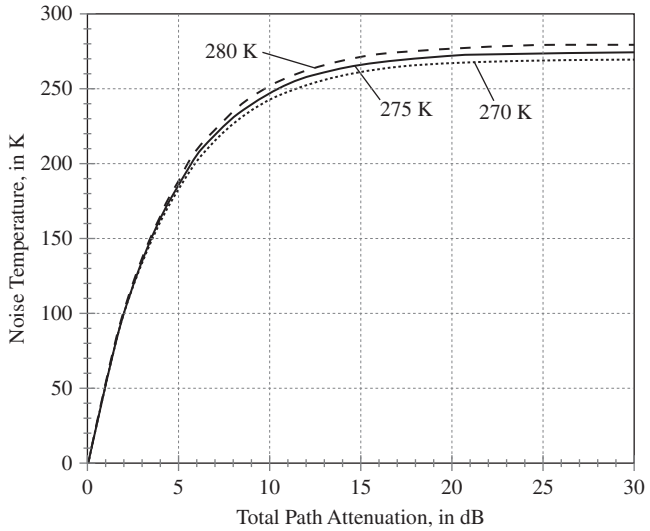

Figure 6.25 Noise temperature as a function of total path attenuation, for mean path temperatures of 270, 275, and 280 K.

www.EngineeringBooksPdf.com

rises quickly with attenuation level. It is 56 K for a 1 dB fade, 137 K for a 3 dB fade, and 188 K for a 5 dB fade level.

The noise temperature introduced by rain will add directly to the receiver system noise figure, and will degrade the overall performance of the link. The noise power increase occurs coincident with the signal power decrease due to the rain fade; both effects are additive and contribute to the reduction in link carrier to noise ratio.

6.5.4 Sky Noise Due to Clouds

Sky noise from clouds can be determined from radiative transfer approximations in much the same way as given in the previous section for sky noise from rain. The temperature and cloud absorption coefficient variations along the path must be defined, and Eqs. 6.33 through 6.34 can be applied.

Slobin (1982) [10] provided calculations of cloud attenuation and cloud noise temperature for several locations in the United States, using radiative transfer methods and a four-layer cloud model. Table 6.2 summarizes the zenith (90° elevation angle) sky noise temperature as calculated by Slobin for several frequencies of interest. Cloud temperatures for other elevation angles can be estimated from

$$t_\theta = \frac{t_z}{\sin\ \theta} \quad 90 \leq \theta \leq 10 \ \text{degrees} \tag{6.41}$$

where t_z is the zenith angle cloud temperature, and t_θ is the cloud temperature at the path elevation angle θ.

Slobin also developed annual cumulative distributions of zenith cloud sky temperature for specified cloud regions at 15 frequencies from 8.5 to 90 GHz. Slobin divided the U.S. into 15 regions of statistically "consistent" clouds as presented in Figure 6.26. The region boundaries are highly stylized and should be interpreted liberally. Some boundaries coincide with major mountain ranges (Cascades, Rockies, and Sierra Nevada), and similarities may be noted between the cloud regions and the rain rate regions of the Global Model. Each cloud region is characterized by observations at a particular National Weather Service observation station. The locations of the observation sites are shown with their three-letter identifiers on the map. For each of these stations, an "average year" was selected on the basis of rainfall measurements. The "average year" was taken to be the one in which the year's monthly rainfall distribution best matched the

Table 6.2 Sky temperature from clouds at zenith (90° elevation angle).

Frequency (GHz)	Light Thin Cloud	Light Cloud	Medium Cloud	Heavy Clouds I	Heavy Clouds II	Very Heavy Clouds I	Very Heavy Clouds II
6/4	< 6°	< 6°	< 13°	< 13°	< 13°	< 19°	< 19°
14/12	6	10	13	19	28	36	52
17	13	14	19	28	42	58	77
20	16	19	25	36	52	77	95
30	19	25	30	56	92	130	166
42	42	52	68	107	155	201	235
50	81	99	117	156	204	239	261

(Source: Ippolito [1]; reproduced by permission of Van Nostrand Reinhold.)

www.EngineeringBooksPdf.com

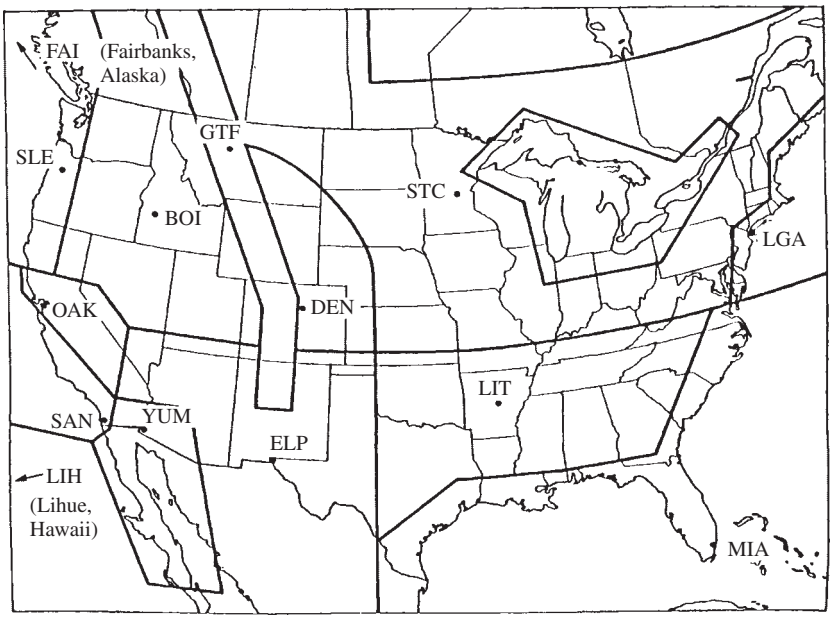

Figure 6.26 Slobin cloud regions. (Source: Slobin [10]; reproduced by permission of American Geophysical Union.)

30-year average monthly distribution. Hourly surface observations for the "average year" for each station were used to derive cumulative distributions of zenith attenuation and noise temperature due to oxygen, water vapor, and clouds.

Figure 6.27(a) through (d), shows examples of zenith sky temperature cumulative distributions for four of the Slobin cloud regions: Denver, New York, Miami, and Oakland, at frequencies of 10, 18, 32, 44, and 90 GHz. Plots for all 15 cloud regions are available in Slobin (1982) [10].

The distributions give the percent of the time the noise temperature is the given value or less. For example, at Denver, the noise temperature was 12 K or less for 0.5 (50%) of the time at 32 GHz. Values of noise temperature in the distribution range 0 to 0.5 (0 to 50%) may be regarded as the range of clear sky conditions. The value of noise temperature at 0% is the lowest value observed for the test year.

Sky temperature values can be approximated from cloud attenuation values by application of Equation 6.35 with t_m, the mean path temperature for clouds, set to 280 K.

6.5.5 Noise From Extra-Terrestrial Sources

Sky noise from sources outside the earth can be present for both uplinks and downlinks, and will depend to a large extent on the included angle of the source and the frequency of operation. The brightness temperature range for the common extraterrestrial noise sources in the frequency range 0.1 to 100 GHz is shown in Figure 6.28.

Above 2 GHz, one need consider only the sun, the moon, and a few very strong non-thermal sources such as Cassiopeia A, Cygnus A and X, and the Crab nebula. The cosmic background contributes only 2.7 K and the Milky Way appears as a narrow zone of somewhat enhanced intensity.

www.EngineeringBooksPdf.com

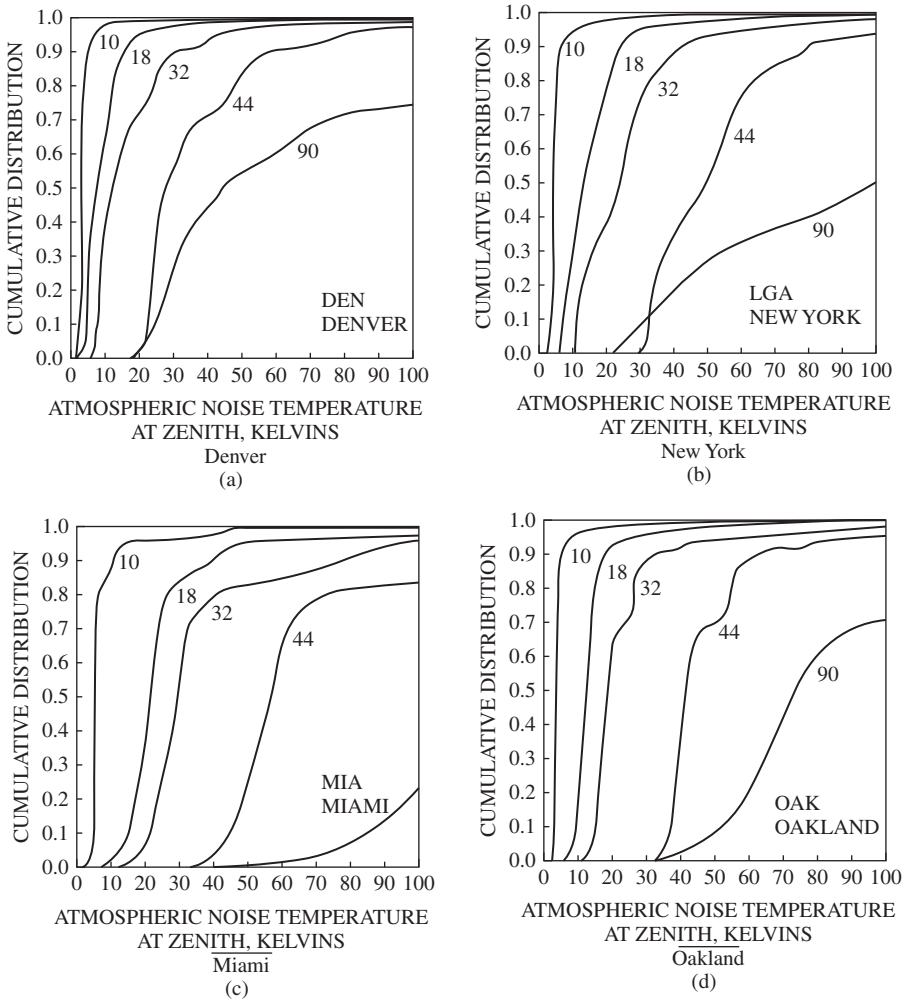

Figure 6.27 Cumulative distributions of zenith sky temperature for four locations from the Slobin cloud model. (Source: Ippolito [1]; reproduced by permission of Van Nostrand Reinhold.)

6.5.5.1 Cosmic Background Noise

Consider first the background noise in the general sky. Figure 6.28 shows that at low frequencies, galactic background noise will be a present, dropping off quickly with frequency up to about 2 GHz.

For communications below 2 GHz, only the sun and the galaxy (the Milky Way), which appears as a broad belt of strong emission, are of concern. For frequencies up to about 100 MHz, the median noise figure for galactic noise, neglecting ionospheric shielding, is given by:

$$NF_m = 52 - 23 \log \ f \tag{6.42}$$

where f is the frequency in MHz

www.EngineeringBooksPdf.com

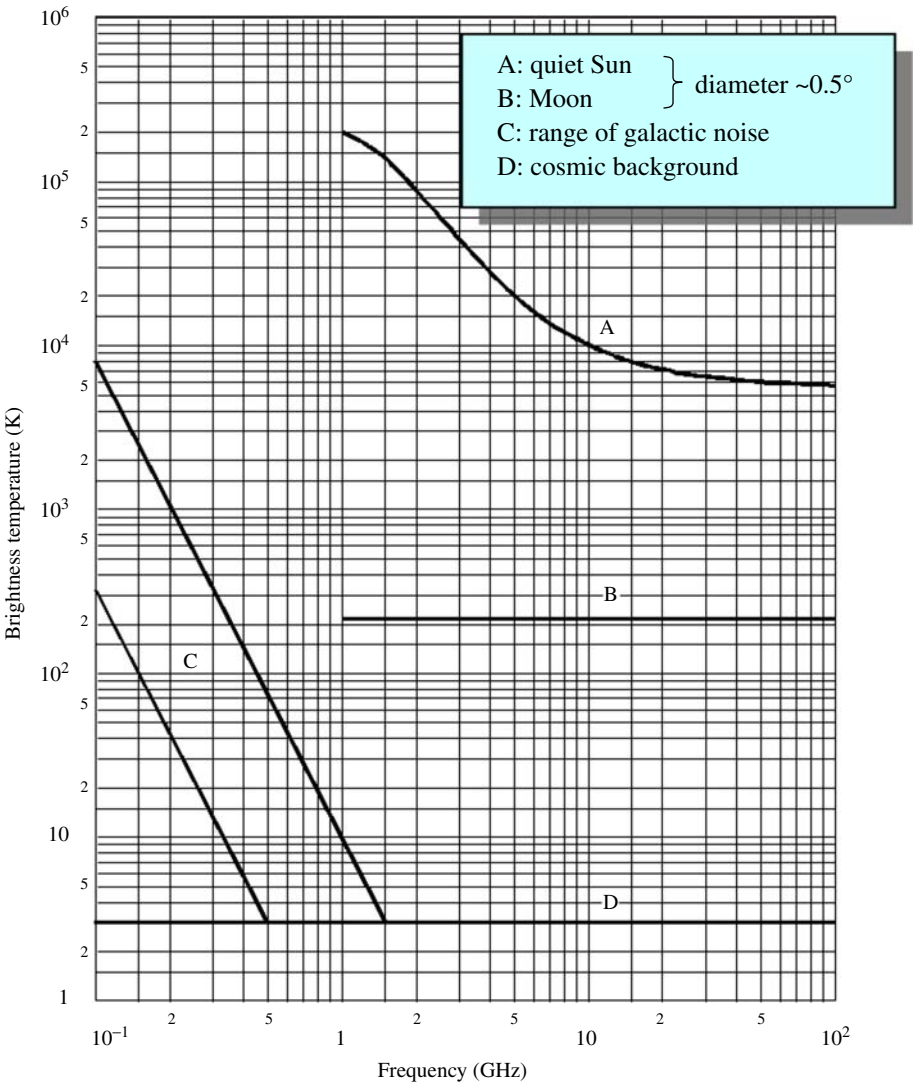

Figure 6.28 Extraterrestrial noise sources. (Source: ITU-R [5]; reproduced by permission of International Telecommunications Union.)

Plots of sky temperature for the Milky Way are provided in Figures 6.29 and 6.30. The plots give the total radio sky temperature at 408 MHz smoothed to 5° angular resolution. The displays are given in equatorial coordinates, declination δ (latitude), and right ascension α (hours eastward around equator from vernal equinox).

The regions displayed in each plot are:

	Right Ascension α	Declination δ
Figure 6.29	0000 h to 1200 h	0° to +90°
Figure 6.30	0000 h to 1200 h	0° to −90°

www.EngineeringBooksPdf.com

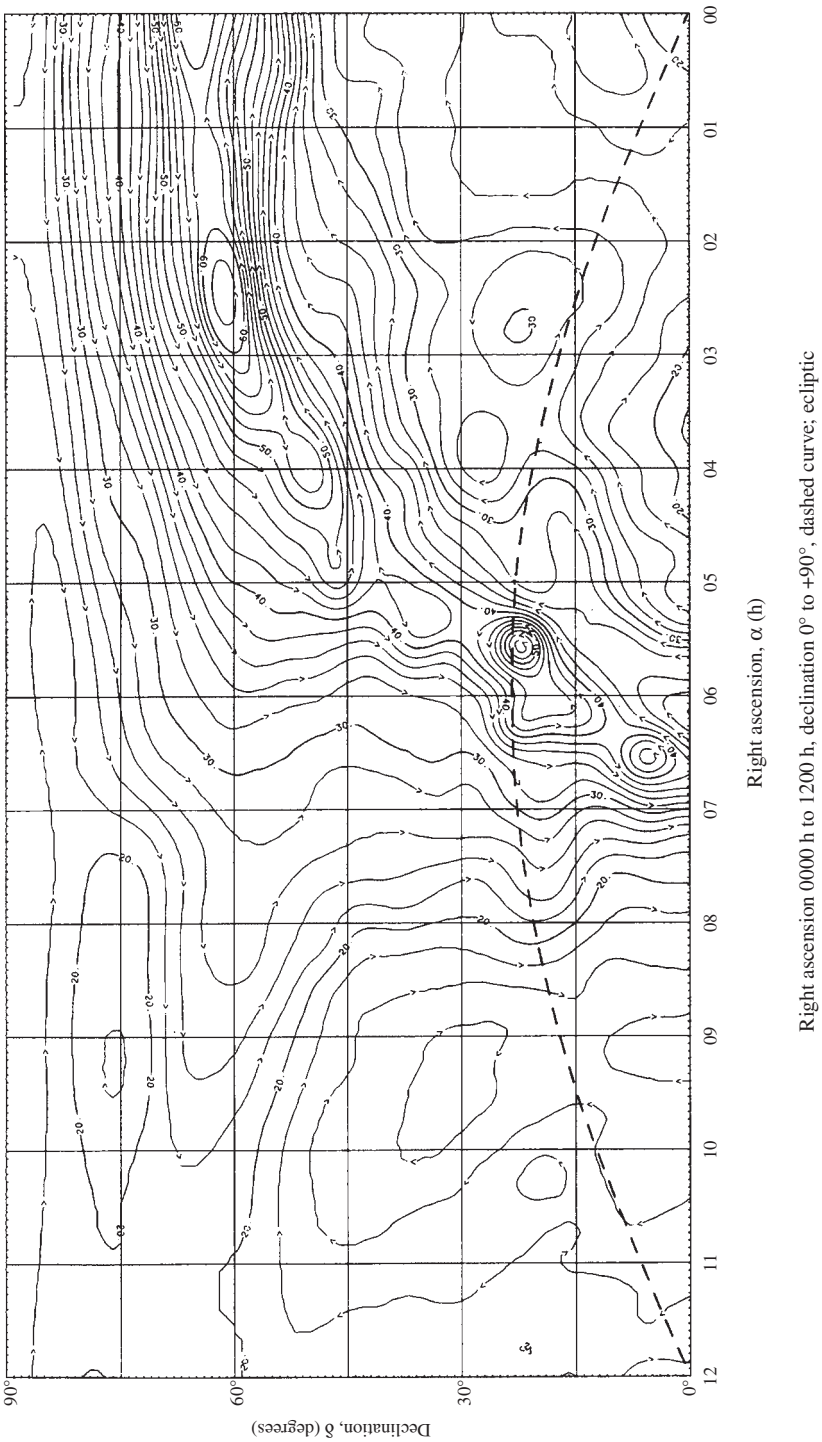

Figure 6.29 Radio sky temperature at 408 MHz. (Source: ITU-R [5]; reproduced by permission of International Telecommunications Union.)

www.EngineeringBooksPdf.com

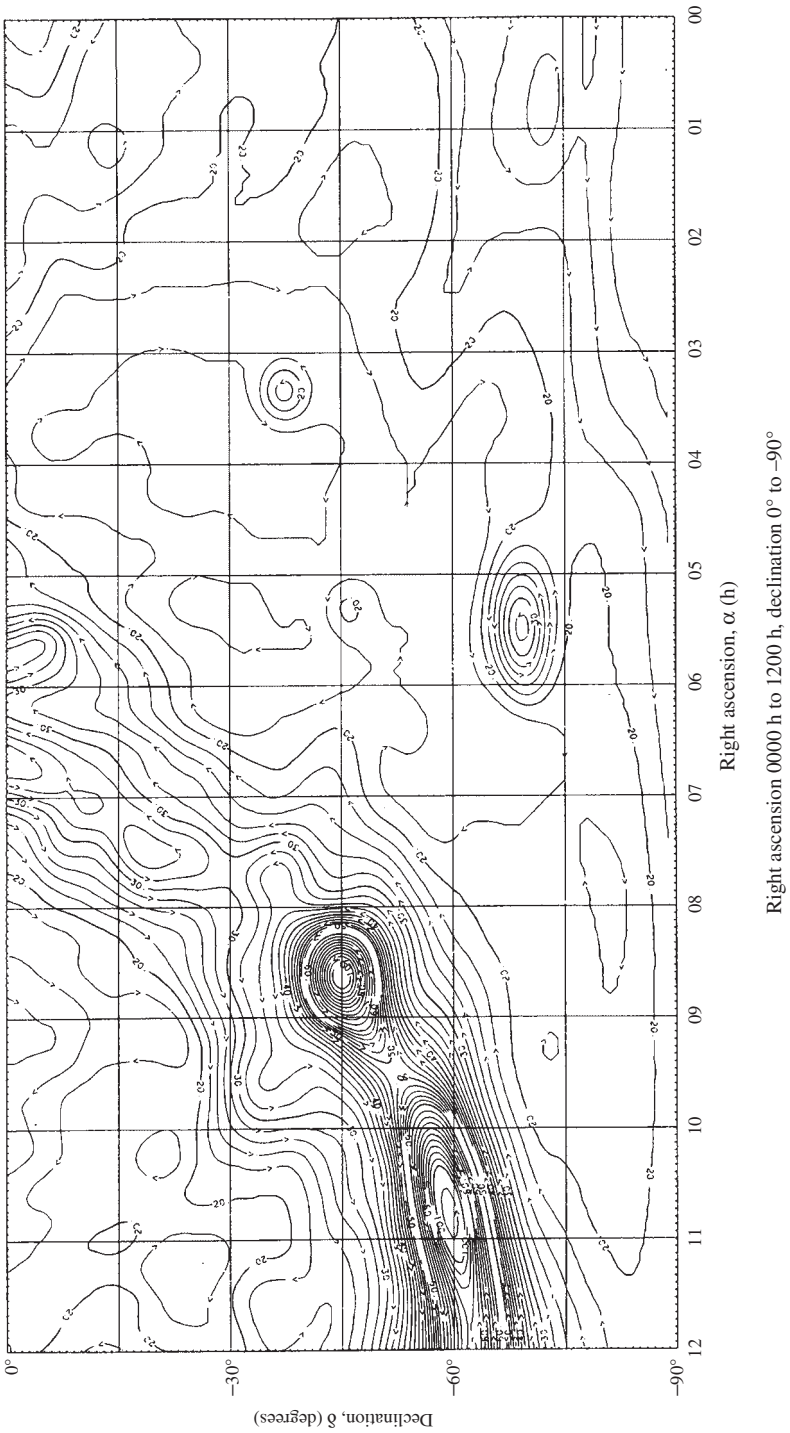

Figure 6.30 Radio sky temperature at 408 MHz. (Source: ITU-R [5]; reproduced by permission of International Telecommunications Union.)

www.EngineeringBooksPdf.com

The contours are directly in K above 2.7 K. The accuracy is 1 K. The contour intervals are:

- 2 K below 60 K,
- 4 K from 60 K to 100 K,
- 10 K from 100 K to 200 K,
- 20 K above 200 K.

Arrows on unlabeled contour lines point clockwise around a minimum in the brightness distribution. The dashed sinusoidal curve between ± 23.5° defines the ecliptic that crosses the Milky Way close to the galactic center. The strongest point sources are indicated by narrow peaks of the temperature distribution, whereas weaker sources are less apparent owing to the limited angular resolution.

An early mapping of cosmic background by Ko & Kraus (1957) [28] provided contour maps of the radio sky for galactic and stellar sources. Figure 6.31 shows a plot of the radio sky at 250 MHz in equatorial coordinates (declination versus right ascension). A geostationary satellite as seen from the Earth appears as a horizontal line of fixed declination between +8.7° and −8.7°, shown by the shaded band on the figure.

The contours of Figure 6.31 are in units of 6 K above 80 K, the values corresponding to the coldest parts of the sky. For example, at 1800 h and 0° declination, the contour value is 37. The brightness temperature at 250 MHz is then $6 \times 37 + 80 = 302$ K. The brightness temperature for another frequency, f_i, is found from

$$t_b(f_i) = t_b(f_o)\left(\frac{f_i}{f_o}\right)^{-2.75} + 2.7 \tag{6.43}$$

For example, the brightness temperature at 1 GHz can be determined from the value of at 250 MHz from:

$$t_b(1\,\text{GHz}) = 302\left(\frac{1}{.25}\right)^{-2.75} + 2.7 = 9.4\,\text{K}$$

At 4 GHz:

$$t_b(4\,\text{GHz}) = 302\left(\frac{4}{.25}\right)^{-2.75} + 2.7 = 2.8\,\text{K}$$

Several relatively strong non-thermal sources, such as Cassiopeia A, Cygnus A and X, and the Crab Nebula are shown on the figure (marked A through D). They are not in the zone of observation for geostationary satellites, and would only be in view for non-geostationary orbits for a very small segment of time.

6.5.5.2 Solar Noise

The sun generates very high noise levels and will contribute significant noise when it is collinear with the Earth station-satellite path. For geostationary satellites, this occurs near the equinoxes, for a short period each day. The power flux density generated by the sun is given as a function of frequency in Figure 6.32 (Perlman, *et al*, 1960 [6.29]). Above about 30 GHz the sun noise temperature is practically constant at 6000 K (Kraus, 1986 [6.30]). The presence of solar noise can be quantitatively represented as an equivalent increase in the antenna noise temperature by an amount t_{sun}. t_{sun} depends on the relative magnitude of the receiver antenna beamwidth compared with the apparent diameter of the sun (0.48°), and how close the sun approaches the antenna boresight. The following

www.EngineeringBooksPdf.com

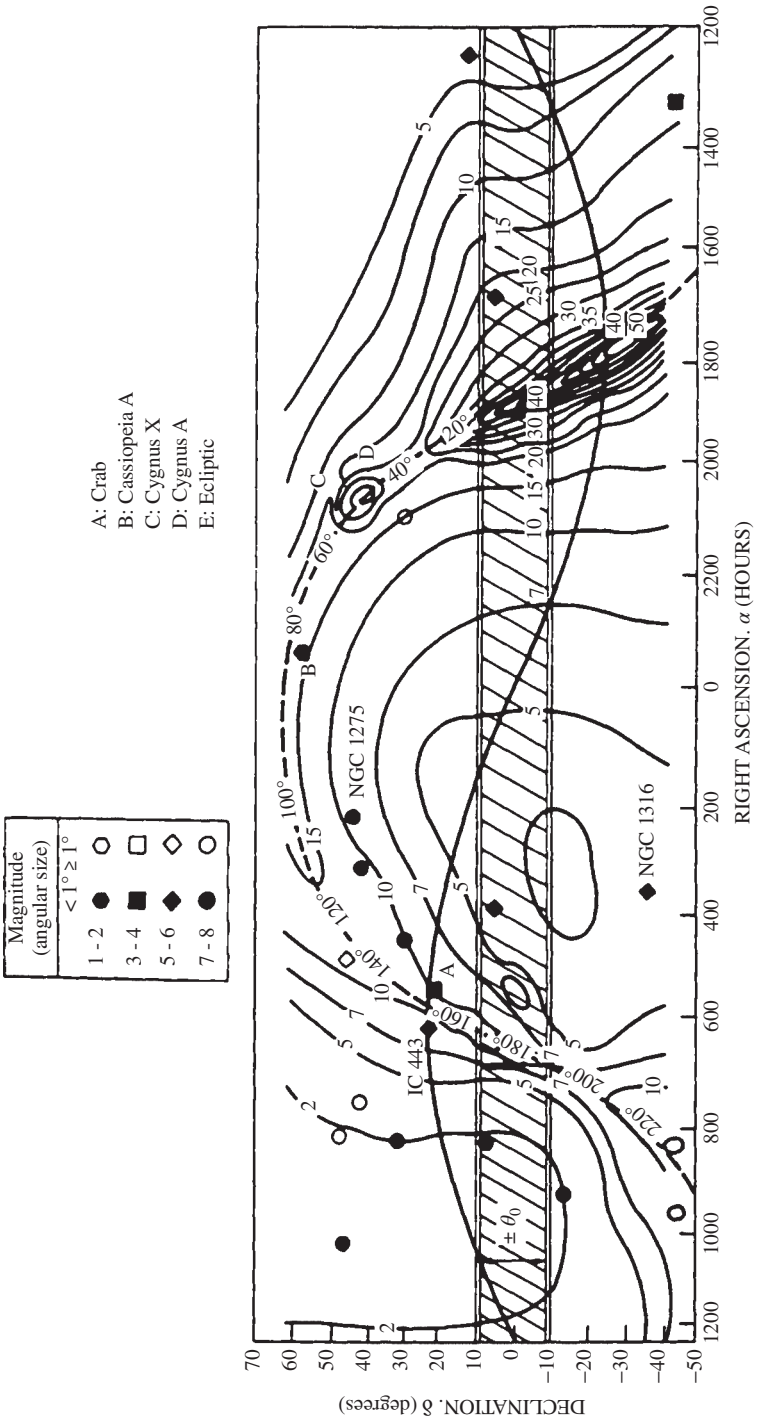

Figure 6.31 The radio sky at 250 MHz in the region around the geostationary orbital arc. (Source: Ippolito [1]; reproduced by permission of Van Nostrand Reinhold.)

www.EngineeringBooksPdf.com

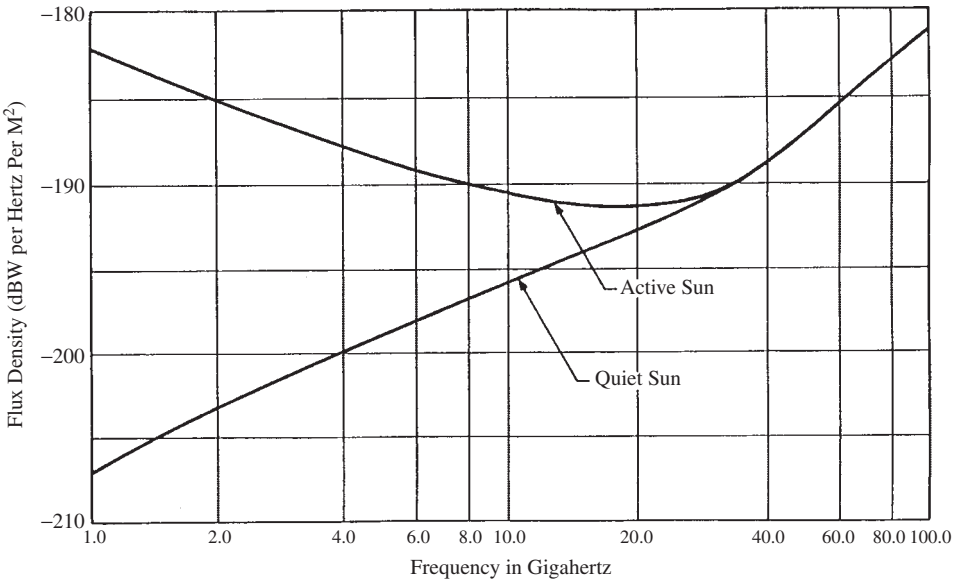

Figure 6.32 Power flux density for quiet and active sun. (Source: Ippolito [28]; reproduced by permission of NASA.)

formula, after Baars (1973) [6.31], gives an estimate of t_{sun} (in degrees K) when the sun, or another extraterrestrial noise source, is centered in the beam.

$$t_{sun} = \frac{1 - e^{-\left(\frac{\delta}{1.20}\right)^2}}{f^2\delta^2} \log^{-1}\left(\frac{S + 250}{10}\right) \tag{6.44}$$

where

δ = apparent diameter of the sun, deg
f = frequency, GHz
S = power flux density, dBw/Hz- m^2
θ = antenna half-power beamwidth, deg

For an Earth station operating at 20 GHz with a 2 meter diameter antenna (beamwidth about 0.5°), the maximum increase in antenna temperature that would be caused by a quiet sun transit is found to be about 8100 K. The sun's flux has been used extensively for measuring tropospheric attenuation. This is done with a sun-tracking radiometer, which monitors the noise temperature of an antenna that is devised to automatically remain pointed at the sun.

6.5.5.3 Lunar Noise

The moon reflects solar radio energy back to the Earth. Its apparent size is approximately 0.5 degrees in diameter, similar to the sun angle. The noise power flux density from the moon varies directly as the square of frequency, which is characteristic of radiation from a "black body." The power flux density from the full moon is about -202 dBW/Hz- m^2 at 20 GHz. The maximum antenna temperature increase due to the moon, for the 20 GHz 2m antenna considered in the previous section, would be 320 K. The phase of the moon and the ellipticity of its orbit cause the apparent size and flux to vary widely, but in

www.EngineeringBooksPdf.com

a regular and predictable manner. The moon has been used to measure Earth station antenna characteristics (Johannsen & Koury, 1974) [32].

6.5.5.4 Radio Stars

The strongest radio stars are ten times weaker than the lunar emission. The strongest stars (Wait *et al.*, 1974) [33] emit typically -230 dBW/Hz- m^2 in the 10 to 100 GHz frequency range. Three of these strong sources are Cassiopeia A, Taurus A, and Orion A. These sources are often utilized for calibration of ground station antenna G/T. During the calibrations the attenuation due to the troposphere is usually canceled out by comparing the sky noise on the star and subtracting the adjacent (dark) sky noise.

References

1 Ippolito LJ. *Radiowave Propagation In Satellite Communications*, Van Nostrand Reinhold, 1986.
2 IEEE *Standard Definitions of Terms for Radio Wave Propagation*, IEEE Std. 211 (New York, August 6, 2002).
3 ITU-R Recommendation P.531–12, "*Ionospheric propagation data and prediction methods required for the design of satellite services and systems*," International Telecommunications Union, Geneva, September 2013.
4 Flock WL. Propagation Effects on Satellite Systems at Frequencies Below 10 GHz, *A Handbook for Satellite Systems Design*, NASA Reference Publication 1108(02), Washington, DC, 1987.
5 ITU-R Recommendation P.372–12, "*Radio Noise*," International Telecom-munications Union, Geneva, July 2015.
6 Mie G. Ann Physik 1908;25:377.
7 Ryde JW, Ryde D. "*Attenuation of centimetere and millimetre waves by rain, hail, fogs, and clouds*," Rep. No. 8670, Research Laboratories of the General Electric Co., Wembley, England, 1945.
8 Gunn KLS, East TWR. The microwave properties of precipitation particles. Quarterly J Royal Meteor Soc 1954;80:522–545.
9 Olsen RL, Rogers DV, Hodge DB. The aR^b relation in the calculation of rain attenuation. IEEE Trans on Antennas and Propagation 1978;AP-26(2):318–329.
10 Slobin SD. Microwave noise temperature and attenuation of clouds: statistics of these effects at various sites in the United States, Alaska, and Hawaii. Radio Science 1982;17(6):1443–1454.
11 ITU-R Recommendation P.840–6, "*Attenuation due to clouds and fog*," International Telecommunications Union, Geneva, September 2013.
12 Chu TS. Rain-Induced Cross-Polarization at Centimeter and Millimeter Wavelengths. The Bell System Technical Journal 1974;53(8):1557–1579.
13 Arnold HW, Cox DC, Hoffman HH, Leck RP. Characteristics of Rain and Ice Depolarization for a 19 and 28 GHz Propagation Path from a Comstar Satellite. IEEE Trans on Antennas and Propagation 1980;AP 28(1):22–28.
14 Nowland WL, Olsen RL, Shkarofsky IP. Theoretical Relationship Between Rain Depolarization and Attenuation. Electronics Letters 1977;13(22):676–678.

www.EngineeringBooksPdf.com

15 Allnutt JE. *Satellite-to-Ground Radiowave Propagation*. Peter Peregrinus Ltd., London, 1989.
16 Vogel WJ. "CTS Attenuation and Cross Polarization Measurements at 11.7 GHz," Final Report, University of Texas, Report No. 22576 1, June 1980.
17 Cox DC, Arnold HW. Results from the 19 and 28 GHZ COMSTAR Satellite Propagation Experiments at Crawford Hill. Proceedings of the IEEE 1982;70(5).
18 ITU-R Recommendation P.453–10, "*The radio refractive index: its formula and refractivity data*," International Telecommunications Union, Geneva, February 2012.
19 Tatarski VE. "*The Effects of the Turbulent Atmosphere on Wave Propagation*," Springfield, VA: National Technical Information Service, 1971.
20 Devasirvathm DJM, Hodge DB. "Amplitude Scintillation of Earth-Space Propagation Paths at 2 and 30 GHz," Ohio State University, Tech. Report 4299–4, March 1977.
21 Titus JM, Arnold HW. "Low Elevation Angle Propagation Effects on COMSTAR Satellite Signals," Bell System Technical Journal, Vol. 61, No. 7, pp. 1567–1572, Sept 1982.
22 Waters JW. "Absorption and Emissions by Atmospheric Gases," *Methods of Experimental Physics, Vol. 12B, Radio Telescopes*. Meeks ML, ed., Academic Press, New York, 1976.
23 Wulfsberg KN. "Apparent Sky Temperatures at Millimeter Wave Frequencies," Phys. Science Res. Paper No. 38, Air Force Cambridge Res. Lab., No. 64,590, 1964.
24 Smith EK. Centimeter and Millimeter Wave Attenuation and Brightness Temperature Due to Atmospheric Oxygen and Water Vapor. Radio Science 1982;17(6):1455–1464.
25 Ippolito LJ. Jr. Effects of precipitation on 15.3 and 31.65 GHz earth space transmissions with the ATS V satellite. Proc of the IEEE 1971;59:189–205.
26 Strickland JI. The measurement of slant path attenuation using radar, radiometers and a satellite beacon. J Res Atmos 1974;8:347–358.
27 Hogg DC, Chu T. The role of rain in satellite communications. Proc of the IEEE 1975;63(9):1308–1331.
28 Ippolito LJ. *Propagation Effects Handbook for Satellite Systems Design*, Fifth Edition, NASA Reference Publication 1082(5), June 1999.
29 Perlman I, *et al.* S potentials and horizontal cells. Proc Natl Acad Sci U S A. 1960;46(5):587–608.
30 Kraus JD. *Radio Astronomy*, 2nd Edition. Cygnus-Quasar Books, 1986.
31 Baars JWM. The Measurement of Large Antennas with Cosmic Radio Sources. IEEE Trans Antennas & Propagat 1973;AP 21(4):461–474.
32 Johannsen KG, Koury A. (1974), The Moon as a Source for G/T Measurements. IEEE Trans Aerospace and Electronic Systems 1974;AES 10(5):718–727.
33 Wait DF, Daywitt WC, Kanda M, Miller CKS. "A Study of the Measurement of G/T Using Casseopeia A," National Bureau of Standards, Report. No. NBSIR 74 382, 1974.

Problems

1 Describe the primary mode of propagation for the following applications:
a) over-the-air HD television

www.EngineeringBooksPdf.com

b) microwave radio relay links
c) over-the-horizon HF communications
d) amateur radio communications
e) air-to-ground VHF communications
f) meteor burst communications
g) satellite-to-hand held mobile terminal links
h) in-building wireless communications

2 Rank the following locations in order of increasing expected ionospheric scintillation for satellite base communications links operating in the L-band: Oslo, Norway; Sao Paolo, Brazil; Sydney, Australia; Rome, Italy; Guam; Tokyo, Japan; and Delhi, India.

3 Determine the Faraday rotation angle for a 1.2 GHz mobile satellite link operating with an average total electron content (TEC) of 10^{17} el/m^2, and an average Earth magnetic field of $5 \times 10\text{-}21$ Webers/m^2. What is the maximum allowable TEC for the above conditions to keep the Faraday rotation below 60 degrees?

4 A shipboard mobile communications terminal operates at an uplink frequency of 1.75 GHz and a downlink frequency of 1.60 GHz. The system is to be sized to allow acceptable operations for any global ocean area location, for any season or time of day, with a minimum elevation angle of 10 degrees. With these requirements in mind, determine the following maximum atmospheric degradations expected for the links, assuming line of site propagation; scintillation index, Faraday rotation, group delay, and differential time delay. The transmission bandwidth is 200 MHz for the uplink and 500 MHz for the downlink. State any assumptions or link conditions used in the evaluation.

5 The level of cloud attenuation rises with increased frequency and with reduced elevation angle. Determine the total cloud attenuation for the following satellite links; a) 20 GHz, 5° elevation angle, b) 74 GHz, 30° elevation angle, c) 30 GHz, 10° elevation angle, d) 44 GHz, 7° elevation angle, and e) 94 GHz, 45° elevation angle. Arrange the results in order of increasing cloud attenuation.

6 The comparative performance of a satellite ground terminal operating in the Washington, DC, area is to be evaluated. The three options for operation are Ku-band, 14.5 GHz uplink/12.25 GHz downlink, Ka-band, 30 GHz uplink/20.75 GHz downlink, and V-band, 50 GHz uplink, 44 GHz downlink. The elevation angle to the satellite is 30°, and the links are to be sized with adequate power margin to insure the link outage will not exceed 1% for an average year. Determine the total atmospheric power margin required for each of the links. Include the contributions of gaseous attenuation, rain attenuation, cloud attenuation, and tropospheric scintillation. Also determine the expected XPD reduction for the same link outage requirements, and the increase in expected sky noise due to each of the atmospheric components. Conclude with an evaluation of the expected performance of the links and the difficulty of achieving the required power margins.

www.EngineeringBooksPdf.com

7 Explain why the noise temperature introduced by rain approaches the mean path temperature of the path for high rain attenuation levels. How does this effect relate to the physical temperature of the ground terminal antenna and the receiver front end hardware?

www.EngineeringBooksPdf.com